Analysis of Drift Instabilities in a Magnetic Nozzle

IEPC-2024-506

Presented at the 38th International Electric Propulsion Conference, Toulouse, France
June 23-28, 2024

Matteo Ripoli* , Mario Merino† and Eduardo Ahedo‡

Department of Aerospace Engineering, Universidad Carlos III de Madrid, Leganés, Spain

Magnetic nozzles are a key component in electrodeless plasma thrusters, acting as their main accelerating device. Non-stationary phenomena common to the entire range of $E \times B$ devices, such as oscillations and instabilities, are believed to be some of the main mechanisms behind anomalous cross-field transport, leading to reduced efficiency. Concurrently, they could be an enabler for electron detachment, necessary for the operation of the device. In this work we present a local linear analysis of fluid instabilities relevant for said devices, expanding on previous works with the addition of plasma inhomogeneities in the direction parallel to the magnetic field, with a rigorous inclusion of magnetic curvature effects, finite Larmor radius effects and 3D wave propagation, allowing for a general formulation of drift-driven instabilities in partially magnetized plasmas. Instability conditions are first studied analytically, and then applied to hybrid PIC/fluid/wave simulation data of a helicon plasma thruster.

I. Introduction

A variety of plasma thrusters operate as partially magnetized $E \times B$ discharges, with electrons closely following magnetic field lines and the heavier ions moving freely from magnetic forces effects. Two notable classes of plasma thrusters are the Hall Thruster (HTs)[1–3] and Electrodeless Plasma Thrusters (EPTs)[4,5] , the latter commonly relying on a Magnetic Nozzle (MN)[6] as their accelerating device. $E \times B$ discharges are known to be subject to oscillations, instabilities, and turbulence,[7] which under certain circumstances lead to non-classical transport of electrons across magnetic field lines, suggesting the existence of additional mechanisms not captured by usual steady-state drift diffusion electron models.

There is ample literature on the study of instabilities through local linear analysis, all sharing the common intention of finding sound physical principles and criteria behind anomalous behaviours in plasmas through a limited but analytically accessible formulation.[8–13] For a two-species Maxwellian plasma at equilibrium, consisting of unmagnetized ions and magnetized electrons, the choice of studying its oscillations by means of either a fluid or a kinetic approach ultimately falls upon the scale of the considered problem. The fluid approach is generally considered valid as long as the perpendicular wavenumber $k_\perp$ times the electron Larmor radius ρ_e is a small number, $k\rho_e < 1$; in the parallel direction, the condition $|k_\parallel c_e| < |\omega_e|$ needs to be respected, with $k_\parallel$, c_e and ω_e the parallel wavenumber, the thermal electron velocity, and the wave frequency in the electron reference frame. This second condition implies that particles moving at thermal velocity parallelly are slower than the wave, so that from an observer moving at the wave phase velocity the plasma behaves as a whole and therefore can be treated as a fluid; at the same time, kinetic paticle-wave interactions such as Landau Damping are neglected. The advantages of employing a fluid approach over a kinetic one lie in its reduced complexity,[14] at the price of assuming *a priori* the aforementioned upper limits on $k_\perp$ and $k_\parallel$.

HT plasmas have been thoroughly studied analytically, numerically and experimentally.[7,13,15–19] Oscillations have been found from the kHz to the tens of MHz ranges. Morozov et al.[20] employed a two-species

*PhD Student, Department of Aerospace Engineering, mripoli@ing.uc3m.es
†Full Professor, Department of Aerospace Engineering, mario.merino@uc3m.es
‡Full Professor, Department of Aerospace Engineering, eahedo@ing.uc3m.es

fluid model with cold, inertialess electrons to justify experimentally observed azimuthally rotating structures. That work is regarded as the first to study the effect of plasma gradients and relative drift between plasma species on the onset of plasma instabilities, which will be referred to as *drift-gradient instabilities*. It was later expanded on by Esipchuk et al.[21] with electron inertia and electromagnetic effects, by Frias et al.[22] with inertialess electrons with the addition of density and temperature gradients, and by Smolyakov et al.[23] with the further inclusion of electron inertia and off-diagonal parts of the electron stress tensor, all of them sharing the common focus on HT plasmas. This last work included the effect of *drift-resistive instabilities* as well, originating from the combination of relative inter-species drift and collisional effects, previously studied by Litvak et al.[24] for both electrostatic and electromagnetic waves. Ramos et al.[11] provided a more general derivation of fluid electrostatic instabilities in $E \times B$ plasmas, examining in detail drift-gradient and drift-dissipative instabilities in a variety of frequency and wavelength regimes along with *stream instabilities*, a class of unstable phenomena uniquely driven by relative drift between species, first presented by Bunemann.[25]

Among the few works including wave propagation both along and across magnetic field lines, the one of Krall[26] from 1971 stands out. In the context of general $E \times B$ discharges, his proposed kinetic model was able to recover in the negligible Larmor radius limit ($k_\perp \rho_e \ll 1$) results known from fluid theory plus a stream instability driven by parallel propagation.

In the case of MNs and EPTs, not much work has been carried out in the analysis of their unsteady behaviour yet. Recent experimental works have suggested the presence of both azimuthal oscillations extending up to the hundreds of kHz[27,28] and azimuthal-axial oscillations.[29,30] Desjardins et al.[31] observe mainly-azimuthal fluctiations in geometrically-comparable linear plasma devices, in the kHz range. Various candidate frameworks have been proposed to explain these phenomena, from the destabilization of electrostatic lower hybrid waves[29] to the magnetosonic wave,[32] the latter being electromagnetic in nature. In [31], the oscillations are identified as a mixture of drift-resistive electron drift waves and Kelvin-Helmoltz instabilities.

The naming conventions of instabilities in partially magnetized plasmas are abundant, and at times conflicting. Two main labelling categories can be identified, relevant to two different frequency regimes: the Electron Cyclotron Drift Instability (ECDI[13,19]), relevant to frequencies comparable to harmonics of the electron gyrofrequency in the electron frame, and Lower-Hybrid Drift Instabilities (LHDI[23,29,33]), relevant instead to frequencies close to the lower-hybrid frequency. Notable fluid limits of the latter are the drift-gradient Modified Simon-Hoh Instability (MSHI[23]) and the Modified Two-Stream Instability (MTSI[26]).

What stands out from the existing body of work on $E \times B$ discharges is that many of the identified instabilities are particular limits of a more general dispersion relation. In fact, it can be stated that a whole family of *fluid* instabilities stem from the presence of a non-zero interspecies drift, be it gradient-driven or otherwise, allowing the presence of 'slow waves with phase velocity smaller then the drift velocity, or, in other terms, with negative Doppler-shifted frequency. These waves are described as carrying negative energy:[34] when coupled with an energy sink—either a positive energy wave or a dissipative process such as inelastic collisions—they can become unstable.[35]

All of the above is based on a 1D description of equilibrium gradients, as it is the relevant case in HTs, Penning and magnetron discharges. In this work we derive a novel formulation for electrostatic drift waves, taking into account inertial, gyroviscous, collisional and 2D gradients as well as 3D wave propagation, conditions relevant to MNs and EPTs. The derivation is carried out in a fluid framework, assuming cold, unmagnetized ions and warm electrons. We will assume long wavelengths, $k_\perp \rho_e < 1$ and $|k_\parallel c_e| < |\omega_e|$. We further assume our plasma to have isotropic temperature at equilibrium and our oscillations to be isothermal.

We focus on the low-mid frequency range $\omega_{ci} \ll \omega < \omega_{ce}$, with ω_{cs} being the cyclotron for the s-th species (i = ions, e = electrons), and work with power expansions on the small parameter $\rho_e/L \ll 1$, with L being the shortest local characteristic equilibrium length. As a novelty in our approach, the resulting system of algebraic equations is solved by iterating on this small parameter. An *a priori* choice has to be made on the order of magnitude of the inertial terms with respect to the cyclotron terms, i.e. whether the electron Doppler-shifted frequency $\omega_e \equiv \omega - \boldsymbol{k} \cdot \boldsymbol{u}_{e0}$ is comparable with ω_{ce} or if $\omega_e = \omega_{ce}\, O(\rho_e/L)$. We will refer to the former choice as to the 'High-Frequency' (HF) regime, while to the latter as the 'Low-Frequency' (LF) one, a differentiation similar to that presented in [11].

The obtained dispersion relation is then applied to input data from pre-existing hybrid PIC/fluid/wave MN simulations, in order to investigate the eventual triggering for instabilities in these devices. The findings are qualitatively contrasted with available experimental data.

The rest of the paper is structured as follows: in section II we will show the general derivation procedure of the dispersion relation in the two frequency regimes, and we will obtain the detailed formulation of the LF one, comparing it with formulations found in literature. In section III we will show analytical solutions of the LF dispersion relation, expressing general instability criteria for both drift-gradient and drift-dissipative perturbations. In section IV we will specialize the dispersion relation to a simulated MN plasma using the data from Jimenez et al.[36,37] as input for the equilibrium plasma quantities and gradients. Finally, in section V we will present a summary and discuss the main findings of this work.

II. The dispersion relation

This section presents the derivation of the local, linear, electrostatic dispersion relation for an $E \times B$ two-fluid plasma composed of cold, unmagnetized ions i, and warm, magnetized electrons e. The model retains perpendicular and parallel gradients, wave propagation in all three directions, and collisional phenomena.

We next work in the context of an axisymmetric MN, with the axis of symmetry coinciding with the z axis. We define the local coordinate system $\{\mathbf{1}_\parallel, \mathbf{1}_\perp, \mathbf{1}_\theta\}$, with $\mathbf{1}_\parallel = \boldsymbol{B}/B$, $\mathbf{1}_\theta$ perpendicular to the (z,r) meridian plane, and $\mathbf{1}_\perp = \mathbf{1}_\theta \times \mathbf{1}_\parallel$. Due to the zeroth-order axisymmetry of the discharge, gradients of the zeroth-order quantities are contained in the $(\mathbf{1}_\parallel, \mathbf{1}_\perp)$ plane.

Being our model fluid, we limit the normalized perpendicular wavenumber to values $k_\perp \rho_{e0} < 1$, with $\rho_{e0} = c_{e0}/\omega_{ce0}$ the electron gyroradius at equilibrium, ω_{ce0} the equilibrium electron gyrofrequency, $c_{e0} \equiv \sqrt{T_{e0}/m_e}$ the equilibrium electron thermal velocity, T_{e0} the (isotropic) equilibrium electron temperature (in eV), m_e the electron mass. For the same reason, in the parallel direction, where motion of electron particles is essentially the free thermal drift, the wavelength must be larger than the distance covered by a single particle during an oscillation, a condition which can be expressed as $|k_\parallel c_{e0}| < |\omega_e|$. We introduce the reference small parameter, $\epsilon = \rho_e/L$, with L the smallest reference equilibrium length in our plasma.

A. General electron equations

Warm, magnetized electrons are described by their continuity and momentum equations, which read:

$$\frac{\partial n_e}{\partial t} + \nabla \cdot (n_e \boldsymbol{u}_e) = \nu_P n_e, \tag{II.1}$$

$$\frac{\partial \boldsymbol{u}_e}{\partial t} + \boldsymbol{u}_e \cdot \nabla \boldsymbol{u}_e = -\frac{\nabla \cdot P_e}{m_e n_e} - \frac{e}{m_e}\left(-\nabla\phi + \boldsymbol{u}_e \times \boldsymbol{B}\right) - \nu_e \boldsymbol{u}_e, \tag{II.2a}$$

where ν_P represents the particle production rate, ϕ the electrostatic potential, ν_e is used to model dissipative forces on the electrons coming from collisional phenomena, and P_e the complete electron pressure tensor including the gyroviscous contribution.

Each quantity Q in the equations above is expended as a zeroth order, time independent part, plus a first order contribution, through which we will model any oscillatory phenomena,

$$Q(\boldsymbol{x}, t) = Q_0(\boldsymbol{x}) + Q_1(\boldsymbol{x}) \exp(i(\boldsymbol{k} \cdot \boldsymbol{x} - \omega t)) + CC, \tag{II.3}$$

with $\boldsymbol{x} = s_\perp \mathbf{1}_\perp + s_\parallel \mathbf{1}_\parallel$ and with the subscripts 0 and 1 referring to equilibrium values and their first order corrections, respectively. The nomenclature CC serves as a reminder that complex conjugates need to be added to recover a real quantity; in the following it is omitted for brevity. It is easy to check that the first order terms of the gradient of Q is composed of two contributions,

$$i\boldsymbol{k} Q_1 + \nabla Q_1, \tag{II.4}$$

with $|\nabla \ln Q_1| = k\ O(\epsilon)$.

B. Zeroth-order equilibrium

In this work, the zeroth order equilibrium plasma quantities and gradients are taken from the hybrid PIC/fluid simulations of the MN of a helicon plasma thruster, presented in [36, 37] The full detail of the model, its numerical implementation, and the results can be found in that work and references therein.

These simulations implement essentially the same electron equations as above, except that they drop electron inertia terms in equation (II.2a), consider a scalar electron pressure $P_{e0} = p_{e0} I$ with $p_{e0} = n_{e0} T_{e0}$, and implement an energy equation for the electron temperature T_{e0}, together with a heat flux closure. Ions and neutrals are treated kinetically as macroparticles.

C. First-order perturbation equations

We next model the first order electrostatic ($B_1 = 0$) perturbations. For simplicity, we shall model the CGL part of the pressure tensor as an isotropic, isothermal scalar pressure, $P_{e1} = p_{e1} I + \Pi_{e1}$, with $p_{e1} = n_{e1} T_{e0}$ and $T_{e1} = 0$. Here, Π_e is the gyroviscous tensor. The zeroth and first order terms of the divergence of Π_e, relevant in the following, are given in appendix A.

In linearized perturbed form, the continuity equation (II.1) for electrons reads, then:

$$-i\omega n_{e1} + n_0 \left(\nabla \cdot \boldsymbol{u}_{e1} + \boldsymbol{u}_{e1} \cdot \nabla \ln n_0\right) + \boldsymbol{u}_{e0} \cdot \nabla ne1 + n_{e1} \nabla \cdot \boldsymbol{u}_{e0} = \nu_P n_{e1} \ . \tag{II.5}$$

Defining the Doppler-shifted frequency as $\omega_e \equiv \omega - \boldsymbol{k} \cdot \boldsymbol{u}_{e0}$ and the normalized number density $h_{e1} \equiv n_{e1}/n_{e0}$, and rearranging terms, this becomes:

$$\begin{aligned} &-i\omega_e h_{e1} + \boldsymbol{u}_{e0} \cdot \nabla h_{e1} + i\boldsymbol{k} \cdot \boldsymbol{u}_{e1} + \nabla_\perp u_{e\perp 1} + \nabla_\parallel u_{e\parallel 1} \\ &\qquad - u_{e\perp 1} \nabla_\perp \ln B_0 - u_{e\parallel 1} \nabla_\parallel \ln B + \boldsymbol{u}_{e1} \cdot \nabla \ln n_0 = -h_{e1} \left(\frac{\nabla \cdot (n_0 \boldsymbol{u}_{e0})}{n_0} - \nu_P \right) \ . \end{aligned} \tag{II.6}$$

The first order electron momentum equation (II.2a), projected along $\mathbf{1}_\perp, \mathbf{1}_\theta, \mathbf{1}_\parallel$, yields:

$$\begin{aligned} &u_{e\perp 1} \left[-i\omega_e + \nu_e + \boldsymbol{u}_{e0} \cdot \nabla \ln u_{e\perp 1} + \nabla_\perp u_{e\perp 0} - \left(\nabla_\parallel \ln B\right) u_{e\parallel 0}\right] + u_{e\theta 1} \omega_{ce0} \\ &\qquad + u_{e\parallel 1} \left[\nabla_\parallel u_{e\perp 0} - \left(\nabla_\parallel \ln B_0\right) u_{e\perp 0} + 2 \left(\nabla_\perp \ln B_0\right) u_{e\parallel 0}\right] = \\ &\quad - \frac{ik_\perp p_{e1} + \nabla_\perp p_{e1}}{m_e n_0} - \frac{\nabla \cdot \Pi_{e1}}{m_e n_0} \cdot \mathbf{1}_\perp + \left(\frac{\nabla_\perp p_{e0}}{m_e n_0} + \frac{\nabla \cdot \Pi_{e0}}{m_e n_0} \cdot \mathbf{1}_\perp \right) h_{e1} + \left(ik_\perp + \nabla_\perp \ln \phi_1\right) \frac{e\phi_1}{m_e} \ , \end{aligned} \tag{II.7a}$$

$$\begin{aligned} &u_{e\perp 1} \left[-\omega_{ce0} + \nabla_\perp u_{e\theta 0}\right] + u_{e\theta 1} \left[-i\omega_e + \nu_e + \boldsymbol{u}_{e0} \cdot \nabla \ln u_{e\theta 1}\right] + u_{e\parallel 1} \nabla_\parallel u_{e\theta 0} = \\ &\qquad - \frac{ik_\theta p_{e1}}{m_e n_0} - \frac{\nabla \cdot \Pi_{e1}}{m_e n_0} \cdot \mathbf{1}_\theta + \frac{\nabla \cdot \Pi_{e0}}{m_e n_0} h_{e1} \cdot \mathbf{1}_\theta + ik_\theta \frac{e\phi_1}{m_e} \ , \end{aligned} \tag{II.7b}$$

$$\begin{aligned} &u_{e\perp 1} \left[-2 \left(\nabla_\parallel \ln B_0\right) u_{e\perp 0} + \nabla_\perp u_{e\parallel 0} - \left(\nabla_\perp \ln B_0\right) u_{e\parallel 0}\right] \\ &\qquad + u_{e\parallel 1} \left[-i\omega_e + \nu_e + \nabla_\parallel u_{e\parallel 0} - \left(\nabla_\perp \ln B_0\right) u_{e\perp 0}\right] + \boldsymbol{u}_{e0} \cdot \nabla u_{e\parallel 1} = \\ &\quad - \frac{ik_\parallel p_{e1} + \nabla_\parallel p_{e1}}{m_e n_0} - \frac{\nabla \cdot \Pi_{e1}}{m_e n_0} \cdot \mathbf{1}_\parallel + \left(\frac{\nabla_\parallel p_{e0}}{m_e n_0} + \frac{\nabla \cdot \Pi_{e0}}{m_e n_0} \cdot \mathbf{1}_\parallel \right) h_{e1} + \left(ik_\parallel + \nabla_\parallel \ln \phi_1\right) \frac{e\phi_1}{m_e} . \end{aligned} \tag{II.7c}$$

Equations (II.6) to (II.7c) can be cast in matrix form for the first order form of the amplitudes, $\boldsymbol{Q}_e = [u_{e\perp}, u_{e\theta}, u_{e\parallel}, h_e]^T$, as

$$A_e \boldsymbol{Q}_{e1} = \left(\boldsymbol{K}^{(0)} + \boldsymbol{K}^{(1)} \right) \frac{e\phi_1}{m_e} \ , \tag{II.8}$$

where $\boldsymbol{K}^{(0)} = i \left[k_\perp, k_\theta, k_\parallel, 0\right]^T$ and $\boldsymbol{K}^{(1)} = \left[\nabla_\perp \ln \phi_1, 0, \nabla_\parallel \ln \phi_1, 0\right]^T$. The 4×4 matrix A_e depends on zeroth order plasma quantities, their gradients and on the gradients of their first order perturbations, symbolically written as $A_e = A_e \left(\omega_s, \boldsymbol{k}, \boldsymbol{Q}_{e0}, \nabla \boldsymbol{Q}_{e0}, \nabla \boldsymbol{Q}_{e1}\right)$. This matrix can be expanded in terms of the small parameter ϵ:

$$\left(A_e^{(0)} + A_e^{(1)} + ... \right) \boldsymbol{Q}_{e1} = \left(\boldsymbol{K}^{(0)} + \boldsymbol{K}^{(1)} \right) \frac{e\phi_1}{m_e} \tag{II.9}$$

so that $A_e^{(n+k)} = A_e^{(n)} O\left(\epsilon^k\right)$. For the first two terms of the expansion, $A_e^{(0)}$ and $A_e^{(1)}$, their dependencies will be

$$A_e^{(0)} = A_e^{(0)} \left(\omega, \boldsymbol{k}, \boldsymbol{Q}_{e0}\right) \ , \qquad A_e^{(1)} = A_e^{(1)} \left(\omega, \boldsymbol{k}, \nabla \boldsymbol{Q}_{e0}, \nabla \boldsymbol{Q}_{e1}\right) \ , \tag{II.10}$$

so that all gradient terms are contained in $A_e^{(1)}$.

This expansion must be continued until the retained A_e matrix is invertible, so that $\boldsymbol{u}_{e1}$ and h_{e1} can be obtained as linear functions of ϕ_1.

If ω_e is of the same order of magnitude of ω_{ce0}, $A_e^{(0)}$ is invertible. Then, we can compute the 'dominant' part of $\boldsymbol{Q}_{e1}$, noted as $\boldsymbol{Q}_{e1}^{(0)}$, as

$$\boldsymbol{Q}_{e1}^{(0)} = \left(A_e^{(0)}\right)^{-1} \boldsymbol{K}^{(0)} \frac{e\phi_1}{m_e}; \tag{II.11}$$

from this, we can compute its derivative in a generic direction x_k (appearing in $A_s^{(1)}$) through the differential form:

$$\frac{\partial \boldsymbol{Q}_{e1}^{(0)}}{\partial x_k}\left(\phi_1, \omega, \boldsymbol{k}, \boldsymbol{Q}_{e0}\right) = \frac{\partial \boldsymbol{Q}_{e1}^{(0)}}{\partial \phi_1}\frac{\partial \phi_1}{\partial x_k} + \sum_{\substack{Q_{e0}\in\{n_0,\\ T_{e0},B_0,\boldsymbol{u}_{e0}\}}} \frac{\partial \boldsymbol{Q}_{e1}^{(0)}}{\partial Q_{e0}}\frac{\partial Q_{e0}}{\partial x_k} \tag{II.12}$$

and we can obtain the full expression of $\boldsymbol{Q}_{e1}$, accurate to the $O(\epsilon)$ order:

$$\boldsymbol{Q}_{e1} = \boldsymbol{Q}_{e1}^{(0)} + \left(A_e^{(0)}\right)^{-1} \boldsymbol{K}^{(1)} \frac{e\phi_1}{m_e} - \left(A_e^{(0)}\right)^{-1} A_e^{(1)} \boldsymbol{Q}_{e1}^{(0)} \ . \tag{II.13}$$

However, if ω_e much smaller of ω_{ce0}, namely $\omega_e = O(\omega_{ce0}\,\epsilon)$, then $A_e^{(0)}$ is singular and the computation of $\boldsymbol{Q}_{e1}$ requires direct inversion of equation (II.8). In this case, the first order quantity gradients can be computed by assuming a weakly inhomogeneous plasma, neglecting second order spatial derivatives of any Q_{e0} and Q_{e1}:

$$\frac{\partial \boldsymbol{Q}_{e1}}{\partial x_k}\left(\phi_1, \omega, \boldsymbol{k}, \boldsymbol{Q}_{e0}, \nabla\boldsymbol{Q}_{e0}, \nabla\boldsymbol{Q}_{e1}\right) \simeq \frac{\partial \boldsymbol{Q}_{e1}}{\partial \phi_1}\frac{\partial \phi_1}{\partial x_k} + \sum_{\substack{Q_{e0}\in\{n_0,\\ T_{e0},B_0,\boldsymbol{u}_{e0}\}}} \frac{\partial \boldsymbol{Q}_{e1}}{\partial Q_{e0}}\frac{\partial Q_{e0}}{\partial x_k} \ , \tag{II.14}$$

so that $A_e \simeq A_e\left(\omega, \boldsymbol{k}, \boldsymbol{Q}_{e0}, \nabla\boldsymbol{Q}_{e0}\right)$ and $\boldsymbol{Q}_{e1}$ can be expressed as a function of ϕ_1 and A_e alone.

The zeroth-order drift velocity $u_{e\theta 0}$ is one of the relevant parameters for the expansion. In equilibrium, $u_{e\theta 0}$ results from the sum of an $E \times B$ drift and a diamagnetic drift, as shown in 11. Two limiting cases will be analysed: a High-Frequency (HF) one one where $u_{e\theta 0} = O(c_{e0})$ and $\omega_e = O(\omega_{ce})$, relevant for the ECDI, and a a Low-Frequency (LF) one where $u_{e\theta 0} = O(c_{e0}\,\epsilon)$ and $\omega_e = O(\omega_{ce}\,\epsilon)$, relevant for LHDI. Their equilibrium parallel velocity, on the other hand, will be assumed to be at most in the order of the ion sound speed, $|u_{e\|0}| \leqslant O(c_{s0})$, with $c_{s0} \equiv \sqrt{T_{e0}/m_i}$ the ion sound speed and m_i the ion mass.

For the HF case, $A_e^{(0)}$ is invertible; however, for the LF case, presented next,$A_e^{(1)}$ needs to be kept to be able to invert equation (II.8).

D. Ion solution

Cold, unmagnetized, singly-charged ions are described by the same equations (II.1) to (II.2a), neglecting the magnetic force ($B = 0$), pressure tensor ($P_i = 0$), and collisional phenomena ($\nu_i = 0$). Otherwise, the same procedure as above applies, mutatis mutandi (e.g. substituting e with i).

Ion motion at equilibrium is of order $u_{i0} \leqslant O(c_{s0})$, consistently with other studies and observations of MNs[38,39,40]. For ions, $A_i^{(0)}$ is invertible, and the dominant solution $\boldsymbol{Q}_{i1}^{(0)}$ is (neglecting $A_i^{(1)}$ terms)

$$\boldsymbol{u}_{i1}^{(0)} = \frac{\boldsymbol{k}}{\omega_i}\frac{e\phi_1}{m_i} \ , \tag{II.15a}$$

$$h_{i1}^{(0)} = \frac{k^2}{\omega_i^2}\frac{e\phi_1}{m_i} \ . \tag{II.15b}$$

E. Construction of the dispersion relation

Once h_{i1} and h_{e1} have been found as functions of ϕ_1, a closure relation for ϕ_1 is needed. One possibility is, naturally, to employ Poisson's equation, here expanded up to the $O(\epsilon)$ order:

$$-\nabla^2\phi_1 = \left[k^2 - (2ik_\perp - \nabla_\perp \ln B)\nabla_\perp \ln\phi_1 - \left(2ik_\parallel - \nabla_\parallel \ln B\right)\nabla_\parallel \ln\phi_1\right]\phi_1 = \frac{n_0 e}{\varepsilon_0}\left(h_{i1} - h_{e1}\right) \ , \quad \text{(II.16)}$$

with ε_0 the vacuum dielectric permittivity. Though the definition of the plasma frequency of the s-th species,

$$\omega_{ps} = \sqrt{\frac{n_0 e^2}{m_s \varepsilon_0}} \quad (s = i, e) \ , \quad \text{(II.17)}$$

we can see that at the leading order in ϵ, substituting of equation (II.15) in (II.16) yields

$$k^2\left(\frac{1}{\omega_i^2} - \frac{1}{\omega_{pi}^2}\right)\frac{e\phi_1}{m_i} = h_{e1} \quad \text{(II.18)}$$

Alternatively, the system can be closed with the assumption of quasineutrality, which is just the $\varepsilon_0 \to 0$ limit of equation (II.16), i.e. $h_{i1} = h_{e1}$. This is also the limit found for $\omega_{pi}^2 \gg \omega_i^2$ in equation (II.18), and hence we shall use this for the low frequency dispersion relation.

F. Low frequency dispersion relation

In this limit case, ω_e and u_{e0} are of order $O(\epsilon)$ with respect to ω_{ce} and c_e respectively: this makes $A_e^{(0)}$ singular, so that $A_e^{(1)}$ has to be considered for the system to be solved as a function of ϕ_1. Recalling the conditions for the validity our model, we impose the upper limits on the perpendicular wavenumber $k_\perp \rho_e < 1$ and on the parallel wavenumber $|k_\parallel c_e| < |\omega_e|$; this last condition, in the present case, implies $|k_\parallel \rho_e| \leqslant O(\epsilon)$. In the following, we drop the subscript 0 on magnetic field and temperature for brevity, so that $B \equiv B_0$, $T_e \equiv T_{e0}$, $\omega_{ce} \equiv \omega_{ce0}$ and $c_e \equiv c_{e0}$.

With the chosen ordering for u_{e0}, the inertial convective terms appear as $O(\epsilon^2)$ terms and are therefore neglected; then, making use of the following definitions:

$$\omega_\perp \equiv \omega_e - \frac{k_\theta c_e^2}{2\omega_{ce}}\nabla_\perp \ln\left(\frac{p_{e0}}{B^2}\right) \ , \qquad \omega_\parallel \equiv \omega_e - \frac{k_\theta c_e^2}{\omega_{ce}}\nabla_\perp \ln\left(\frac{p_{e0}}{B^4}\right) \ , \quad \text{(II.19)}$$

which are the Doppler-shifted frequencies multiplying the velocity in the directions perpendicular and parallel to the magnetic field respectively, accounting for gyroviscous cancellation.[41] The linearized electron system becomes:

$$-i\left[\omega_\perp + i\nu_e\right]u_{e\perp 1} + \left[\omega_{ce}\left(1 - \frac{k^2\rho_e^2}{2}\right) + i\frac{k_\perp c_e^2}{\omega_{ce}}\nabla_\perp \ln\left(\frac{\sqrt{p_{e0}}u_{e\theta 1}}{B}\right)\right]u_{e\theta 1}$$
$$+ i\frac{k_\theta c_e^2}{\omega_{ce}}\left[ik_\parallel + \nabla_\parallel \ln\left(\frac{p_{e0}u_{e\parallel 1}}{B^{5/2}}\right)\right]u_{e\parallel 1} + c_e^2\left[ik_\perp + \nabla_\perp \ln h_{e1}\right]h_{e1} = \left[ik_\perp + \nabla_\perp \ln\phi_1\right]\frac{e\phi_1}{m_e} \ , \quad \text{(II.20a)}$$

$$-\left[\omega_{ce}\left(1 - \frac{k^2\rho_e^2}{2}\right) + i\frac{k_\perp c_e^2}{\omega_{ce}}\nabla_\perp \ln\left(\frac{\sqrt{p_{e0}}u_{e\perp 1}}{B}\right)\right]u_{e\perp 1} - i\left[\omega_\perp + i\nu_e\right]u_{e\theta 1}$$
$$- i\frac{k_\perp c_e^2}{\omega_{ce}}\left[ik_\parallel + \nabla_\parallel \ln\left(\frac{p_{e0}u_{e\parallel 1}}{B^{5/2}}\right)\right]u_{e\parallel 1} + ic_e^2 k_\theta h_{e1} = ik_\theta \frac{e\phi_1}{m_e} \ , \quad \text{(II.20b)}$$

$$-i\frac{k_\theta c_e^2}{\omega_{ce}}\left[ik_\parallel + \nabla_\parallel \ln\left(\sqrt{B}u_{e\perp 1}\right)\right]u_{e\perp 1} + i\frac{k_\perp c_e^2}{\omega_{ce}}\left[ik_\parallel + \nabla_\parallel \ln\left(\sqrt{B}u_{e\theta 1}\right)\right]u_{e\theta 1} - i\left[\omega_\parallel + i\nu_e\right]u_{e\parallel 1}$$
$$+ c_e^2\left[ik_\parallel + \nabla_\parallel \ln h_{e1}\right]h_{e1} = \left[ik_\parallel + \nabla_\parallel \ln\phi_1\right]\frac{e\phi_1}{m_e} \ , \quad \text{(II.20c)}$$

$$\left[ik_\perp + \nabla_\perp \ln\left(\frac{n_0 u_{e\perp 1}}{B}\right)\right] u_{e\perp 1} + ik_\theta u_{e\theta 1} + \left[ik_\parallel + \nabla_\parallel \ln\left(\frac{n_0 u_{e\parallel 1}}{B}\right)\right] u_{e\parallel 1} - i\omega_e h_{e1} = 0 \ . \tag{II.20d}$$

Keeping only leading order terms, the determinant D_e of the above system is

$$D_e = -\omega_{ce}^2 \left(\omega_\parallel + i\nu_e\right) \left\{ \omega_e \left(1 - \frac{k^2\rho_e^2}{2}\right)^2 - \frac{k_\theta c_{e\perp}^2}{\omega_{ce}} \left[\nabla_\perp \ln\left(\frac{n_0 u_{e\perp 1}}{B}\right) - \nabla_\perp \ln h_{e1}\right] \left(1 - \frac{k^2\rho_e^2}{2}\right) \right.$$
$$\left. + k^2\rho_e^2 \left(\omega_\perp + i\nu_e\right) + \rho_e^2 k_\perp^2 \frac{k_\theta c_{e\perp}^2}{\omega_{ce}} \nabla_\perp \ln\left(\frac{u_{e\perp 1}}{u_{e\theta 1}}\right) - \frac{R_\parallel}{\omega_\parallel + i\nu_{e\parallel}} \right\} , \tag{II.21}$$

where we have defined

$$R_\parallel = -c_e^2 \left[\left(ik_\parallel + \ell_\parallel + \ell_n\right) \left(1 + \frac{k^2\rho_e^2}{2}\right) + \ell_T k^2 \rho_e^2 \right]$$
$$\times \left[\left(ik_\parallel + \nabla_\parallel \ln h_{e1}\right) \left(1 - \frac{k^2\rho_e^2}{2}\right) + ik_\parallel k^2\rho_e^2 + \ell_\perp k_\theta^2 \rho_e^2 + \ell_\theta k_\perp^2 \rho_e^2 \right] , \tag{II.22}$$

with

$$\ell_\perp = \nabla_\parallel \ln\left(\sqrt{B} u_{e\perp 1}\right) \ , \quad \ell_\theta = \nabla_\parallel \ln\left(\sqrt{B} u_{e\theta 1}\right) \ , \quad \ell_\parallel = \nabla_\parallel \ln\left(\frac{u_{e\parallel 1}}{\sqrt{B}}\right) \ ,$$
$$\ell_n = \nabla_\parallel \ln\left(\frac{n_0}{\sqrt{B}}\right) \ , \qquad \ell_T = \nabla_\parallel \ln\left(\frac{T_e}{\sqrt{B^3}}\right) \ . \tag{II.23}$$

We can now compute h_{e1} keeping only leading order terms:

$$\frac{D_e h_{e1}}{e\phi_1/m_e} = \frac{D_e}{c_e^2} + \frac{\omega_{ce}^2}{c_e^2} \left(1 - \frac{k^2\rho_e^2}{2}\right) \left(\omega_\parallel + i\nu_e\right) \left[\omega_e \left(1 - \frac{k^2\rho_e^2}{2}\right) + \frac{k_\theta c_e^2}{\omega_{ce}} \nabla_\perp \ln\left(\frac{h_{e1}}{\phi_1}\right) \right]$$
$$+ \omega_{ce}^2 \left(1 - \frac{k^2\rho_e^2}{2}\right) \left[\left(\ell_\parallel + \ell_n\right) \left(1 - \frac{k^2\rho_e^2}{2}\right) + \left(\ell_\parallel + \ell_n + \ell_T\right) k^2\rho_e^2 \right] \nabla_\parallel \ln\left(\frac{h_{e1}}{\phi_1}\right) \ ; \tag{II.24}$$

Now, neglecting second order spatial derivatives, we can simplify the following algebra through $|\nabla\omega_{ce}| \gg |\nabla\omega_e|$. Then, from equation (II.14) the gradient of D_e can be approximated as:

$$\nabla D_e \approx 2 \left(\nabla \ln B\right) D_e \ . \tag{II.25}$$

The gradient of $\ln h_{e1}$ is:

$$\nabla \ln h_{e1} = \nabla \ln\left(\frac{D_e h_{e1}}{e\phi_1/m_e}\right) - \nabla \ln D_e + \nabla \ln \phi_1 \simeq \nabla \ln \phi_1 \ . \tag{II.26}$$

Accordingly, equation (II.24) simplifies to:

$$\frac{D_e h_{e1}}{e\phi_1/m_e} = \frac{D_e}{c_e^2} + \frac{\omega_{ce}^2}{c_e^2} \left(1 - \frac{k^2\rho_e^2}{2}\right)^2 \left(\omega_\parallel + i\nu_e\right) \omega_e \ , \tag{II.27}$$

while yielding for the velocities (keeping only leading order terms):

$$\frac{D_e u_{e\perp 1}}{e\phi_1/m_e} = i\omega_{ce} \left(1 - \frac{k^2\rho_e^2}{2}\right) \left(\omega_\parallel + i\nu_e\right) k_\theta \omega_e \ , \tag{II.28a}$$

$$\frac{D_e u_{e\theta 1}}{e\phi_1/m_e} = -i\omega_{ce} \left(1 - \frac{k^2\rho_e^2}{2}\right) \left(\omega_\parallel + i\nu_e\right) k_\perp \omega_e \ , \tag{II.28b}$$

$$\frac{D_e u_{e\parallel 1}}{e\phi_1/m_e} = i\omega_{ce}^2 \left(1 - \frac{k^2\rho_e^2}{2}\right) \left[\left(ik_\parallel + \nabla_\parallel \ln\phi_1\right) \left(1 - \frac{k^2\rho_e^2}{2}\right) + ik_\parallel k^2\rho_e^2 + \ell_\perp k_\theta^2 \rho_e^2 + \ell_\theta k_\perp^2 \rho_e^2 \right] \omega_e \ . \tag{II.28c}$$

As in equation (II.26), equations. (II.28a) to (II.28c) allow us to compute the gradients of each velocity component:

$$\nabla \ln u_{e\perp 1} = \nabla \ln u_{e\theta 1} = -\nabla \ln B + \nabla \ln \phi_1 \ , \tag{II.29a}$$

$$\nabla \ln u_{e\parallel 1} = \nabla \ln \phi_1 \ . \tag{II.29b}$$

The above relations imply:

$$\ell_\perp = \ell_\theta = \ell_\parallel = \nabla_\parallel \ln \phi_1 - \frac{\nabla_\parallel \ln B}{2} \ , \tag{II.30}$$

while $R_\parallel$ (equation (II.22)) becomes:

$$\begin{aligned} R_\parallel = -c_e^2 \Bigg\{ \left[\left(ik_\parallel + \nabla_\parallel \ln \left(\frac{n_0 \phi_1}{B} \right) \right) \left(1 + \frac{k^2 \rho_e^2}{2} \right) - \frac{\nabla_\parallel \ln B}{2} k^2 \rho_e^2 \right] + k^2 \rho_e^2 \nabla_\parallel \ln \left(\frac{T_e}{B} \right) \Bigg\} \\ \times \Bigg\{ \left[\left(ik_\parallel + \nabla_\parallel \ln \left(\frac{n_0 \phi_1}{B} \right) \right) \left(1 + \frac{k^2 \rho_e^2}{2} \right) - \frac{\nabla_\parallel \ln B}{2} k^2 \rho_e^2 \right] - \nabla_\parallel \ln \left(\frac{n_0}{B} \right) \left(1 + \frac{k^2 \rho_e^2}{2} \right) \Bigg\} \ . \end{aligned} \tag{II.31}$$

Recalling the definition of $\omega_\perp$ from equation (II.19), the determinant can finally be rewritten as

$$\begin{aligned} D_e = -\omega_{ce}^2 \left(\omega_\parallel + i\nu_e \right) \Bigg\{ \omega_e \left(1 + \frac{k^4 \rho_e^4}{4} \right) - \frac{k_\theta c_e^2}{\omega_{ce}} \left[\nabla_\perp \ln \left(\frac{n_0}{B^2} \right) + k^2 \rho_e^2 \nabla_\perp \ln T_e \right] \\ + i\nu_e k^2 \rho_e^2 - \frac{R_\parallel}{\omega_\parallel + i\nu_e} \Bigg\} \ . \end{aligned} \tag{II.32}$$

By defining the following frequencies:

$$\omega_{Me} \equiv -\frac{k_\theta c_e^2}{\omega_{ce}} \nabla_\perp \ln \left(\frac{n_0}{B^2} \right) \ , \qquad \omega_{Te} \equiv -\frac{k_\theta c_e^2}{\omega_{ce}} \nabla_\perp \ln T_e \ , \tag{II.33}$$

and by coupling equation (II.27) with equation (II.15) through quasineutrality we get, keeping only leading order terms and by neglecting every $O(\epsilon)$ order term, the following dispersion relation:

$$\begin{aligned} 0 = \left[\frac{k^2}{\omega_i^2} \frac{e}{m_i} - \frac{e}{m_e c_e^2} \frac{\omega_{Me} + k^2 \rho_e^2 \left(\omega_e + \omega_{Te} + i\nu_e \right) - R_\parallel / \left(\omega_\parallel + i\nu_e \right)}{\omega_e + \omega_{Me} + k^2 \rho_e^2 \left(\omega_{Te} + i\nu_e \right) + k^4 \rho_e^4 \omega_e / 4 - R_\parallel / \left(\omega_\parallel + i\nu_e \right)} \right] \phi_1 \\ \equiv f\left(\omega_i, \boldsymbol{k} \right) \phi_1 . \end{aligned} \tag{II.34}$$

Being $R_\parallel$ complex, the relation $\omega_i = \omega_i(\boldsymbol{k})$ becomes in turn complex $\forall \boldsymbol{k} \in \mathbb{R}$ even in the absence of collisions ($\nu_e = 0$). Physically, were $\mathrm{Im}\left\{ R_\parallel \right\} \neq 0$, it could either imply that *a*) the parallel gradients either act as power sources or sinks for the instability, destabilizing the flow across the entire k spectrum, or that *b*) the described instability is apparent, that is, an otherwise stable wave moving through a spatial envelope, transforming a *spatial* amplification (or decay) to a *temporal* amplification (or decay).[42]

Only for one value of $\nabla_\parallel \ln \left(n_0 \phi_1 / B \right)$, that is,

$$\nabla_\parallel \ln \left(\frac{n_0 \phi_1}{B} \right)^{ref} \equiv \frac{1}{2} \left[\nabla_\parallel \ln \left(\frac{n_0}{B} \right) - \nabla_\parallel \ln \left(\frac{T_e}{B^2} \right) \frac{k^2 \rho_e^2}{1 + k^2 \rho_e^2 / 2} \right] \tag{II.35}$$

does the dispersion relation $f(\omega_i, \boldsymbol{k}) = 0$ admit real values of ω_i as solutions in the collisionless case, being $R_\parallel$ completely real:

$$R_\parallel = c_e^2 \left(1 + \frac{k^2 \rho_e^2}{2} \right)^2 \left\{ k_\parallel^2 + \frac{1}{4} \left[\nabla_\parallel \ln \left(\frac{n_0}{B} \right) + \frac{k^2 \rho_e^2}{1 + k^2 \rho_e^2 / 2} \nabla_\parallel \ln \left(\frac{T_e}{B} \right) \right]^2 \right\} \ . \tag{II.36}$$

It can be shown that any choice other than (II.35) is equivalent to selecting a frame of reference moving with respect to the one with $\mathrm{Im}\{R_\parallel\} = 0$. Let's choose for example a slightly different shape for $\nabla_\parallel \ln(n_0\phi_1/B)$, say

$$\nabla_\parallel \ln\left(\frac{n_0\phi_1}{B}\right) = \nabla_\parallel \ln\left(\frac{n_0\phi_1}{B}\right)^{ref} + k_i \tag{II.37}$$

with k_i small and real. It is quite easy to see that, upon substitution in equation (II.31), k_i behaves as the imaginary part of the now complex parallel wavenumber $k_\parallel + ik_i$. Then, if $\omega(\boldsymbol{k}) \in \mathbb{R}$ was a stable solution for $k_i = 0$, its new form for $k_i \neq 0$ will be:

$$\omega\left(\boldsymbol{k} + ik_i\mathbf{1}_\parallel\right) \simeq \omega(\boldsymbol{k}) + i\frac{\partial\omega}{\partial k_\parallel}k_i \equiv \omega(\boldsymbol{k}) + iv_{g\parallel}k_i = \omega_r(\boldsymbol{k}) + i\gamma \tag{II.38}$$

with $v_{g\parallel}$ the parallel group velocity in the parallel direction, $\gamma = \mathrm{Im}(\omega)$ and $\omega_r = \mathrm{Re}(\omega)$. It is then a simple exercise to show that selecting $k_i \neq 0$ corresponds to selecting a frame moving with parallel velocity $\mathrm{v}_\parallel = v_{g\parallel}k_i/\left[\nabla_\parallel \ln(n_0\phi_1/B)^{ref}\right] \neq 0$ with respect to the frame with $k_i = 0$. We therefore choose this stable reference frame with $k_i = \mathrm{v}_\parallel = 0$ as the one of interest, continuing with the closure $\nabla_\parallel \ln(n_0\phi_1/B) = \nabla_\parallel \ln(n_0\phi_1/B)^{ref}$.

Substituting equation (II.31) into equation (II.34) and dividing by ϕ_1, the dispersion relation finally renders as:

$$\frac{k^2c_s^2}{\omega_i^2} = \frac{\omega_{Me} + k^2\rho_e^2\left(\omega_e + \omega_{Te} + i\nu_e\right) - R_\parallel/\left(\omega_\parallel + i\nu_e\right)}{\omega_e\left(1 + k^4\rho_e^4/4\right) + \omega_{Me} + k^2\rho_e^2\left(\omega_{Te} + i\nu_e\right) - R_\parallel/\left(\omega_\parallel + i\nu_e\right)} \tag{II.39}$$

with $R_\parallel$ containing effects of both parallel wave propagation and gradients.

Equation (II.39) is clearly akin to equation (31) from [23], with the additions of magnetic field curvature effects, parallel dynamics and plasma inhomogeneities in the $\perp$-$\parallel$ plane.

1. *Notable limits of the low frequency dispersion relation*

From here, two notable limits can be taken: the dispersion relations for MSHI[23] and the MTSI,[26] respectively

$$\frac{k^2c_s^2}{\omega_i^2} = \frac{\omega_{Me}}{\omega_e + \omega_{Me}} \qquad \left(k^2\rho_e^2 \to 0,\ R_\parallel \to 0\right), \tag{II.40}$$

and

$$\frac{k^2c_s^2}{\omega_i^2} = -\frac{c_e^2k_\parallel^2}{\omega_e^2 - c_e^2k_\parallel^2} \qquad \left(k^2\rho_e^2 \to 0,\ \nabla Q_0 \to 0\right), \tag{II.41}$$

both expressed in their quasi-neutral limit.

Lastly, if we assume $\nabla_\parallel \ln Q_0 = 0$, $\nu_\parallel \gg \omega_e$ and $k\rho_e \ll 1$, we recover

$$\frac{k^2c_s^2}{\omega_i^2} = \frac{\omega_{Me} + i\left(k^2\rho_e^2\nu_e + \dfrac{c_e^2k_\parallel^2}{\nu_e}\right)}{\omega_e + \omega_{Me} + i\left(k^2\rho_e^2\nu_e + \dfrac{c_e^2k_\parallel^2}{\nu_e}\right)} \tag{II.42}$$

which is the cold, unmagnetized ion limit of equation (13) from [43].

The first two limits (II.40)-(II.41) express the two main ingredients for stream and drift gradient instabilities, which are interspecies drifts due to gradients (in the perpendicular direction) or due to different thermal velocties (in the parallel direction), as will be later shown in section III.A. The third limit (II.42) shows how the combined presence of drifts and collisions naturally introduces destabilization in the problem by introducing imaginary terms in the dispersion relation, a concept further explored in section III.B. As a summary, these three limits show the building blocks for fluid instabilities that arise in partially magnetized plasmas.

III. Low frequency instabilities

Now, we specialize the quasineutral limit of the dispersion relation obtained in equation (II.39) to the Magnetic Nozzle case, using simulated data from Ref. [36] for the equilibrium plasma quantities and their gradients.

In general, solutions of the dispersion relation $\omega_i = \omega_i(\boldsymbol{k})$ come in two regimes: a higher frequency pair of electron drift waves with $\omega_i \sim \boldsymbol{k}\cdot\boldsymbol{u}_{e0}$, and a lower-hybrid pair, with $\omega_i \sim k\rho_e\omega_{LH}$. This is a framework similar to that analysed in [11] for the 'low-frequency modes in the low-drift regime', with an added fourth branch due to the inclusion of parallel dynamics.

In the collisionless limit, only the lower-hybrid branches experience destabilization in the form of a reactive instability (pair of complex conjugate solutions). In the collisional case, one of the two electron drift waves can be destabilized as well, namely the one with frequency in the electron frame $\omega_e < 0$. The reason, as anticipated in the introduction, has to do with the existence of 'slow' electron waves in presence of zeroth order drifts. In the collisionless case the only energy sinks present in the plasma are ion acoustic waves, whose frequency lies in the ω_{LH} range: when the two types of wave have matching frequencies and wavenumbers, an unstable interaction takes place. When inelastic collisions are present in the medium they act as an energy sink, destabilizing the slow electron wave without the need of coupling with the ion sound wave.

In general, the presence of collisions widens considerably the parametric instability region, while at the same time lowering the growth rates of the drift gradient instabilities identified in the collisionless limit. The analysis is therefore focused mostly on drift-gradient (collisionless) instabilities; notwithstanding this, at the end of this section, a paragraph is dedicated to drift-resistive (collisional) instability conditions and how resistive effects alter the collisionless case.

A. Drift-gradient instabilities

Defining:

$$\Delta \equiv \omega_i - \omega_e = \boldsymbol{k}\cdot(\boldsymbol{u}_{e0} - \boldsymbol{u}_{i0}) \ , \qquad \Delta_\parallel \equiv \omega_i - \omega_\parallel \ , \tag{III.1}$$

the former being the Doppler shift between the two species, equation (II.39) can be hugely simplified by considering either lower-hybrid wave solutions $\omega_i^2 \sim k^2c_s^2 = k^2\rho_e^2\omega_{LH}^2$ or electron drift wave solutions $\omega_i^2 \sim \Delta^2 \gg k^2c_s^2$. Here we are assuming $|u_{e0}| \gg |c_s|$, as expected in current-free MNs.

For the electron drift wave solutions, equation (II.39) approximately becomes

$$\omega_e^2 + \left(\frac{\omega_{Me}}{k^2\rho_e^2} + \omega_{Te} + \Delta - \Delta_\parallel\right)\omega_e + \left(\Delta - \Delta_\parallel\right)\left(\frac{\omega_{Me}}{k^2\rho_e^2} + \omega_{Te}\right) - \frac{R_\parallel}{k^2\rho_e^2} \simeq 0 \tag{III.2}$$

admitting solutions

$$\omega_i = \Delta - \frac{1}{2}\left(\frac{\omega_{Me}}{k^2\rho_e^2} + \omega_{Te} + \Delta - \Delta_\parallel\right)\left[1 \pm \frac{\sqrt{\left[k^2\rho_e^2\left(\Delta - \Delta_\parallel - \omega_{Te}\right) - \omega_{Me}\right]^2 + R_\parallel}}{k^2\rho_e^2\left(\Delta - \Delta_\parallel + \omega_{Te}\right) + \omega_{Me}}\right] \ , \tag{III.3}$$

which are always stable for $R_\parallel \geqslant 0$.

Moving to the lower-hybrid branches, following the assumption $k^2c_s^2 \ll \Delta^2$ and expanding up to the second power of ω_i/Δ, we get

$$\omega_i^2 - \frac{k^2c_s^2\omega_i}{\Delta_\parallel}\frac{\left(\Delta + \Delta_\parallel\right)\left(1 + k^4\rho_e^4/4\right) - \left(\omega_{Me} + k^2\rho_e^2\omega_{Te}\right)}{\omega_{Me} + k^2\rho_e^2\left(\omega_{Te} - \Delta\right) + R_\parallel/\Delta_\parallel} \\ - k^2c_s^2\frac{\Delta\left(1 + k^4\rho_e^4/4\right) - \omega_{Me} - k^2\rho_e^2\omega_{Te} - R_\parallel/\Delta_\parallel}{\omega_{Me} + k^2\rho_e^2\left(\omega_{Te} - \Delta\right) + R_\parallel/\Delta_\parallel} \simeq 0 \tag{III.4}$$

whose solution $\omega_i = \omega_{ir} + i\gamma$ has real and imaginary parts:

$$\omega_{ir} = k^2\rho_e^2\frac{\omega_{LH}^2}{2\Delta_\parallel}\frac{\left(\Delta + \Delta_\parallel\right)\left(1 + k^4\rho_e^4/4\right) - \left(\omega_{Me} + k^2\rho_e^2\omega_{Te}\right)}{\omega_{Me} + k^2\rho_e^2\left(\omega_{Te} - \Delta\right) + R_\parallel/\Delta_\parallel} \ , \tag{III.5}$$

$$\gamma \simeq \omega_{LH}k\rho_e\sqrt{\frac{\Delta\left(1 + k^4\rho_e^4/4\right) - \omega_{Me} - k^2\rho_e^2\omega_{Te} - R_\parallel/\Delta_\parallel}{\omega_{Me} + k^2\rho_e^2\left(\omega_{Te} - \Delta\right) + R_\parallel/\Delta_\parallel}} \ . \tag{III.6}$$

The 38th International Electric Propulsion Conference, P. Baudis Convention Center, Toulouse, France, June 23-28, 2024

The expression for γ allows us to retrieve the following general instability criterion:

$$\left[\Delta\left(1+\frac{k^4\rho_e^4}{4}\right)-\omega_{Me}-k^2\rho_e^2\omega_{Te}-\frac{R_\parallel}{\Delta_\parallel}\right]\left[\omega_{Me}+k^2\rho_e^2\left(\omega_{Te}-\Delta\right)+\frac{R_\parallel}{\Delta_\parallel}\right]>0\ . \tag{III.7}$$

This relation underlines how the electron drifts in the ion reference frame are the ones driving the instability, whether they may be due to *a*) gradients in electrostatic potential, pressure or magnetic field, or *b*) thermal motion along the magnetic field lines.

1. *Long-wavelength limit*

Taking the limit $k\rho_e \to 0$ of relation (III.7), the instability criterion simplifies to:

$$\left[\Delta-\omega_{Me}-\frac{R_\parallel}{\Delta_\parallel}\right]\left[\omega_{Me}+\frac{R_\parallel}{\Delta_\parallel}\right]>0\ . \tag{III.8}$$

This expression can be easily shown to be a generalization of the MSHI and the MTSI conditions, whose relevant dispersion relations expressed at the end of section II. Neglecting parallel propagation and gradients, $R_\parallel = 0$, yields the MSHI criterion

$$\left[\Delta-\omega_{Me}\right]\omega_{Me}>0\ ; \tag{III.9}$$

Instead, dropping perpendicular inhomogeneities ($\omega_{Me}=0$, $\Delta_\parallel=\Delta$) yields the MTSI condition

$$\Delta^2>R_\parallel\ . \tag{III.10}$$

2. *Finite Larmor radius effects*

As $k\rho_e$ becomes non-negligible, rearranging the relation (III.7) yields a finite Larmor radius correction to the criterion in (III.8):

$$\begin{aligned}\left[\Delta-\omega_{Me}-\frac{R_\parallel}{\Delta_\parallel}\right]\left[\omega_{Me}+\frac{R_\parallel}{\Delta_\parallel}\right]>\\ k^2\rho_e^2\Bigg[\left(\omega_{Te}-\frac{k^2\rho_e^2\Delta}{4}\right)\left(\omega_{Me}+\frac{R_\parallel}{\Delta_\parallel}\right)-\left(\omega_{Te}-\Delta\right)\left(\Delta-\omega_{Me}-\frac{R_\parallel}{\Delta_\parallel}\right)\\ +k^2\rho_e^2\left(\omega_{Te}-\frac{k^2\rho_e^2\Delta}{4}\right)\left(\omega_{Te}-\Delta\right)\Bigg]\ ,\end{aligned} \tag{III.11}$$

implying that even if the condition for long-wavelength instabilities are not respected (for instance, left-hand side of (III.11) <0), we can still have an onset for larger values of the normalized wavenumber $k\rho_e$. On the other hand, if the long-wavelength criterion from (III.8) is satisfied, higher values of $k^2\rho_e^2$ might cause ω_i to become real, quenching the instability.

B. Drift-resistive instabilities

Up until now we have considered a collisionless plasma. When collisional effects are included, the dispersion relation becomes a complex polynomial in ω_i, yielding in general complex solutions as a result. To understand the conditions for which at least one solution might yield an unstable growth, we can perform a standard marginal stability analysis,[11] finding out the conditions for which at least one branch admits $\omega_i \in \mathbb{R}$ as a solution, meaning that its imaginary part is changing sign (thus moving to or from a stable configuration to an unstable one).

Supposing then $\omega_i \in \mathbb{R}$ and solving the imaginary part of equation II.39:

$$\left\{\nu_e\left[\omega_{Me}+k^2\rho_e^2\left(\omega_e+\omega_{Te}\right)\right]+k^2\rho_e^2\nu_e\omega_\parallel\right\}\left(\omega_i^2-k^2c_s^2\right)=k^2c_s^2\omega_e\nu_e\left(1-\frac{k^2\rho_e^2}{2}\right)^2\ ; \tag{III.12}$$

solving now the real part:

$$\left\{\omega_{\parallel}\left[\omega_{Me}+k^2\rho_e^2\left(\omega_e+\omega_{Te}\right)\right]-k^2\rho_e^2\nu_e^2-R_{\parallel}\right\}\left(\omega_i^2-k^2c_s^2\right)=k^2c_s^2\omega_e\omega_{\parallel}\left(1-\frac{k^2\rho_e^2}{2}\right)^2 . \tag{III.13}$$

Multiplying both sides by $\left\{\nu_e\left[\omega_{Me}+k^2\rho_e^2\left(\omega_e+\omega_{Te}\right)\right]+k^2\rho_e^2\nu_e\omega_{\parallel}\right\}$ and substituting equation (III.12) into (III.13):

$$\left\{\omega_{\parallel}\left[\omega_{Me}+k^2\rho_e^2\left(\omega_e+\omega_{Te}\right)\right]-\nu_e^2-R_{\parallel}\right\}k^2c_s^2\omega_e\nu_e\left(1-\frac{k^2\rho_e^2}{2}\right)^2=$$
$$\left[\omega_{Me}+k^2\rho_e^2\left(\omega_e+\omega_{\parallel}+\omega_{Te}\right)\right]k^2c_s^2\omega_e\omega_{\parallel}\nu_e\left(1-\frac{k^2\rho_e^2}{2}\right)^2 ; \tag{III.14}$$

in general, equation (III.14) admits only $\omega_e=0$ as a solution for $\nu_e\neq 0$, which in turn implies $\omega_i^2=k^2c_s^2$. This is only ever satisfied by having $\Delta=\pm kc_s$, which indicates that a real solution is only possible for $u_{e0}=\pm c_s$ (assuming $k\simeq|k_\theta|$).

Using analytical continuation,

$$0\simeq f(\omega_i,\boldsymbol{k})\big|_{\nu_e=0}+\frac{\partial f}{\partial\omega_i}\delta\omega_i+\frac{\partial f}{\partial\nu_e}\nu_e \tag{III.15}$$

yields the growth rate due to destabilization from dissipative forces:

$$\delta\omega_i=-\frac{\partial f/\partial\nu_e}{\partial f/\partial\omega_i}\bigg|_{\nu_e=0}\nu_e. \tag{III.16}$$

Computing the partial derivatives, and substituting them into equation (III.16):

$$\delta\omega_i=-\frac{i\nu_e\left(\omega_i^2-k^2c_s^2\right)\left(k^2\rho_e^2+R_{\parallel}/\omega_{\parallel}^2\right)}{2\omega_i\left[\omega_{Me}+k^2\rho_e^2\left(\omega_e+\omega_{Te}\right)-R_{\parallel}/\omega_{\parallel}\right]+\left(k^2\rho_e^2+R_{\parallel}/\omega_{\parallel}^2\right)\left(\omega_i^2-k^2c_s^2\right)-k^2c_s^2\left(1-k^2\rho_e^2/2\right)^2} ; \tag{III.17}$$

taking the limits $\omega_i^2\to k^2c_s^2$ and $\omega_e\to 0$ of equation (III.17) then yields:

$$\gamma=-\nu_e\left(\omega_i^2-k^2c_s^2\right)\frac{k^2\rho_e^2+R_{\parallel}/\omega_{\parallel}^2}{2\omega_i\left[\omega_{Me}+k^2\rho_e^2\omega_{Te}-R_{\parallel}/\omega_{\parallel}\right]-k^2c_s^2\left(1-k^2\rho_e^2/2\right)^2}. \tag{III.18}$$

Using the marginal stability condition $\omega_i\approx\Delta$, $\omega_{\parallel}\approx\Delta-\Delta_{\parallel}$, and assuming $|\omega_{Me}|\gg k^2c_s^2$:

$$\gamma\simeq\nu_e\left(\Delta^2-k^2c_s^2\right)\frac{k^2\rho_e^2+R_{\parallel}/\left(\Delta-\Delta_{\parallel}\right)^2}{k^2c_s^2\left(1-k^2\rho_e^2\right)^2-2\Delta\left[\omega_{Me}+k^2\rho_e^2\omega_{Te}-R_{\parallel}/\left(\Delta-\Delta_{\parallel}\right)\right]}. \tag{III.19}$$

We conclude that, given that $R_{\parallel}\geqslant 0$ for any $k_{\parallel}$ and any combination of parallel gradients, destabilization can happen a) for supersonic drifts ($|\Delta|>kc_s$) when the denominator is negative, or b) for subsonic drifts in the opposite case. However, while dissipative forces in the perpendicular plane can be neglected in the long-wavelength limit ($k\rho_e\to 0$), parallel friction always has to be considered.

For our high-drift case of interest, electron drift waves $|\omega_i|\sim\Delta\gg kc_s$ can be shown to be destabilized when $\omega_e<0$ (substituting equation (III.3) in (III.17)). It can also be shown through equation (III.17) that drift gradient instability growth rates are in general lowered by the added dissipation. From this, we can state that while collisions offer a more general destabilization criterion, they also tend to reduce unstable growths excited by gradients alone.

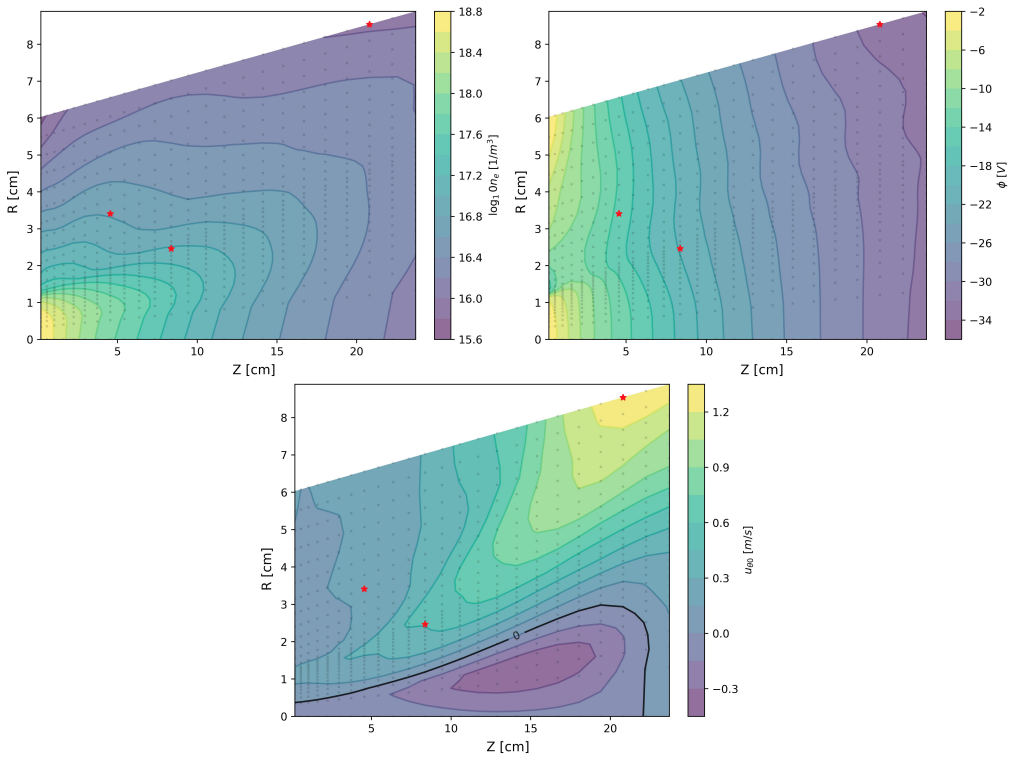

Figure IV.1: Simulation data from Ref. [36]. Contour plots for n_0, ϕ_0 and $u_{e\theta 0}$. The red dots represent the three points for which a ω_i-k plot has been obtained.

IV. Application to MN simulation data

As a means of illustration, in this paragraph, numerical solutions of (II.39) are obtained for each point in the entire 2D map shown in Figure IV.1, stemming from the simulations of the MN of a helicon plasma thruster reported in 36. The simulation data was obtained through a 2D hybrid code, HYPHEN-EPT, with electrons modelled as a magnetized diffusive fluid, while the heavy species are simulated through a PIC formulation,[44,45] and wavefields are solved in the frequency domain using a cold-plasma-wave model.[36]

Three points have been chosen from the shown MN region, two in the near-plume and one in the far-plume part of the discharge, to show three different $\omega_i\,(\boldsymbol{k})$ trends for a drift-gradient instability. Each location shows a different evolution of γ w.r.t., starting from the triggering of a quasi-MSHI in the first case and ending with a short-wavelength instability, mostly driven by parallel dynamics, in the third case. Table 1 shows their coordinates, and associated zeroth-order plasma quantities and gradients.

z [cm]	r [cm]	ω_{LH} [10^6 s^{-1}]	c_s [10^3 m/s]	$u_{e\theta 0}$ [10^5 m/s]	$\nabla_\perp \ln n_0$ [m^{-1}]	$\nabla_\perp \ln B$ [m^{-1}]	$\nabla_\perp \ln T_e$ [m^{-1}]	$\nabla_\parallel \ln\left(\frac{n_0}{B}\right)$ [m^{-1}]	$\nabla_\parallel \ln T_e$ [m^{-1}]
4.5	3.4	8.1	1.9	1.7	−39.4	7.5	−2.5	0.4	−0.0
8.4	2.5	3.2	1.9	4.5	−98.7	2.5	3.2	−1.9	−0.2
20.8	8.5	0.2	1.9	12.7	−23.5	2.2	1.6	0.1	−0.6

Table 1: Coordinates, zeroth-order plasma quantities and gradients at the three reference points.

Figure IV.2 presents the real and imaginary parts of the solution $\omega_i\,(\boldsymbol{k})$ for the near-plume point with axial and radial coordinates $(z, r) = (4.5, 3.4)$ cm. For $k_\parallel/k_\theta = k_\perp/k_\theta = 0$ it presents an instability mainly driven by perpendicular dynamics, respecting the MSHI criterion from equation (III.9) and developing mostly in long-wavelength regime $k\rho_e \ll 1$. The instability disappears for small values of the ratio $k_\parallel/k_\theta$; the effect of $k_\perp$ is on the other hand negligible, leaving the shape of the solution almost unchanged. For this very reason, in this point and in the following ones, the solutions have been plotted with $k_\perp/k_\theta = 0$.

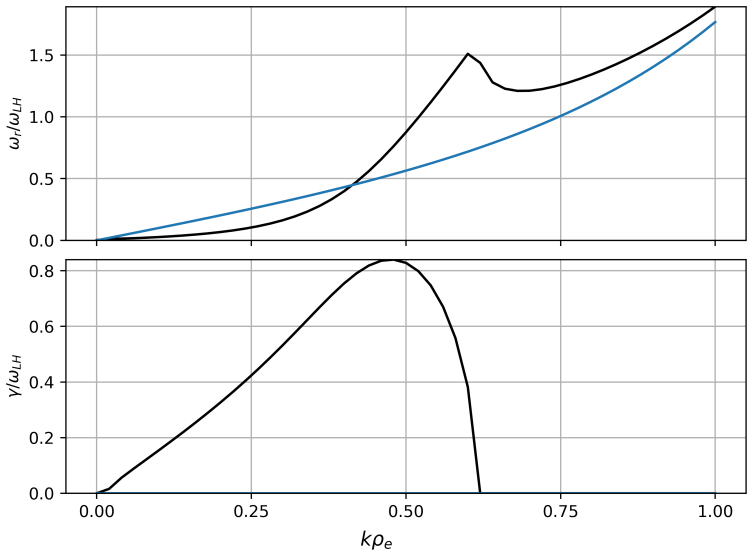

Figure IV.2: Real frequency (top figure) and growth rate (bottom figure) for the long-wavelength destabilization of the lower-hybrid branch for the point of coordinates $(z, r) = (4.5, 3.4)$ cm. Black lines are for $k_\parallel = 0$; blue lines for $k_\parallel/k_\theta = 2 \cdot 10^{-2}$. Relevant zeroth-order plasma quantities and gradients are shown in Table 1.

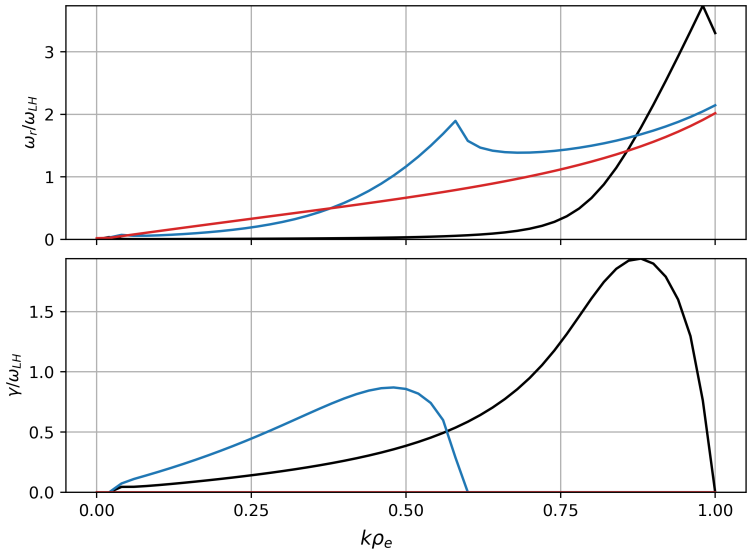

Figure IV.3: Real frequency (top figure) and growth rate (bottom figure) for the destabilized lower-hybrid branch for the point of coordinates $(z, r) = (8.4, 2.5)$ cm, with onset in the long-wavelength regime and peak in the short-wavelength regime. Black lines are for $k_\parallel = 0$; blue lines for $k_\parallel/k_\theta = 2 \cdot 10^{-2}$; red lines for $k_\parallel/k_\theta = 4 \cdot 10^{-2}$. Relevant zeroth-order plasma quantities and gradients are shown in Table 1.

Figure IV.3 shows the destabilized lower-hybrid branch for the point $(z, r) = (8.4, 2.5)$ cm. In this case the MSHI is no longer respected as the perpendicular components of the electric field and density gradient have different sign, so that the inclusion of parallel dynamics is responsible for the destabilization of the lower-hybrid branch. The instability develops at a slight larger $k\rho_e$ but still in the long-wavelength regime. However its peak is reached in the short-wavelength, at $k\rho_e = O(1)$. Once again, $|k_\parallel| > 0$ has a stabilizing effect, separating the ion sound wave and the 'slow' electron wave.

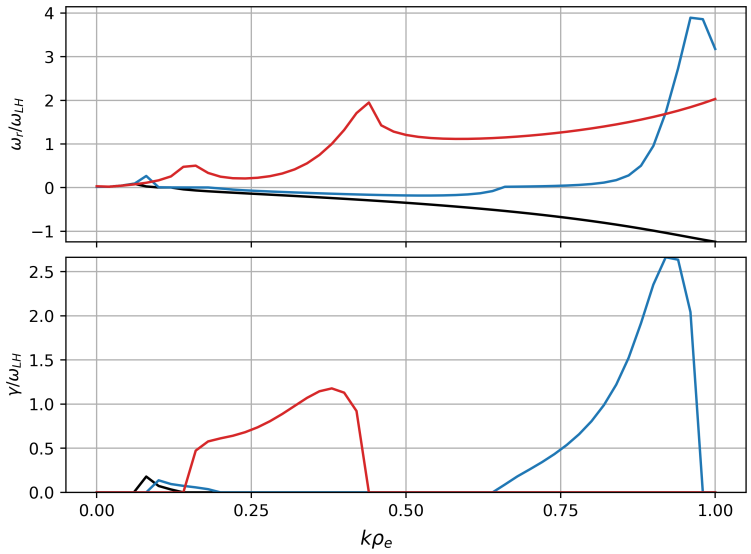

Figure IV.4: Real frequency (top figure) and growth rate (bottom figure) for the short-wavelength destabilization of the lower-hybrid branch for the point of coordinates $(z, r) = (20.8, 8.5)$ cm. Black lines are for $k_\parallel = 0$; blue lines for $k_\parallel/k_\theta = 8 \cdot 10^{-2}$; red lines for $k_\parallel/k_\theta = 16 \cdot 10^{-2}$. Relevant zeroth-order plasma quantities and gradients are shown in Table 1.

Figure IV.4 shows the ω_i-k plot of the unstable lower-hybrid branch at the point $(z, r) = (20.8, 8.5)$ cm. In this case, far from the MSHI condition, the effect of parallel dynamics $R_\parallel/\Delta_\parallel$ is negligible when compared to the large Doppler shift $\Delta \sim k_\theta u_{e\theta 0}$, as shown by the small growth rate peak when $k_\parallel/k_\theta = 0$ (black line). The instability is then driven by finite parallel propagation $|k_\parallel/k_\theta| > 0$, creating a separate short-wavelength onset region as the ratio $|k_\parallel/k_\theta|$ grows (blue line). Eventually, the long and short-wavelength onset regions collapse into a single one for larger values of said ratio (red line).

These three cases have been analysed to apply the concepts and criteria developed in section III on a relevant configuration. We may now move our attention on the study and identification of the most unstable modes developing in a MN, as predicted by our model.

For each point of the map, the maximum growth rate $\gamma_{max} = \max_{\boldsymbol{k},\omega_r} (\gamma(\boldsymbol{k}, \omega_r))$ has been obtained, with the associated wavenumber and real frequency $\boldsymbol{k}^*$, ω_{ir}^* respecting the conditions $\rho_e k^* < 1$ and $|k_\parallel^* c_e| < |\omega_e^*|$. The mode associated with $\gamma = \gamma_{max}$ is then the most unstable for that particular point of the nozzle; 2D maps of γ_{max}, ω_{ir}^* and $\boldsymbol{k}^*$ are shown in Figure IV.5.

The regions with larger γ_{max} are mostly found in those same points where $|u_{e\theta 0}|$ reaches its peaks. This can be explained by looking at the relation between γ and Δ from equation (III.6), with $\gamma \lesssim \sqrt{\Delta}$ and by noting that, in general, $\Delta\left(\omega_{Me} + R_\parallel/\Delta_\parallel\right) > 0$. A similar consideration can be done with the plot of ω_{ir}^*, recalling the expression of ω_{ir} from equation (III.5), and with the plot of $k_\theta^* \rho_e$, as $\Delta \propto k_\theta$. All these first three plots show very similar trends, as they all share a direct correlation with the Doppler shift Δ and the zeroth-order electron drift velocity $u_{e\theta 0}$. The ratio $k_\parallel^*/k_\theta^*$ is quite negligible in the near plume. As we've stated in the discussion of the three ω_i-k plots, in this region the effect of a finite parallel propagation is, in general, to stabilize the wave. This is not true in the $u_{e\theta 0} < 0$ region and in the far-plume region, as shown in Figure IV.4. The role of $k_\perp^*$, on the other hand, is quite marginal, as we've stated beforehand. It follows a trend more or less similar to that of $k_\parallel^*$, peaking in a region of small γ_{max}.

In those points where γ_{max} is reached for $k^* \rho_e = 1$, a kinetic formulation of the problem would be more suitable.

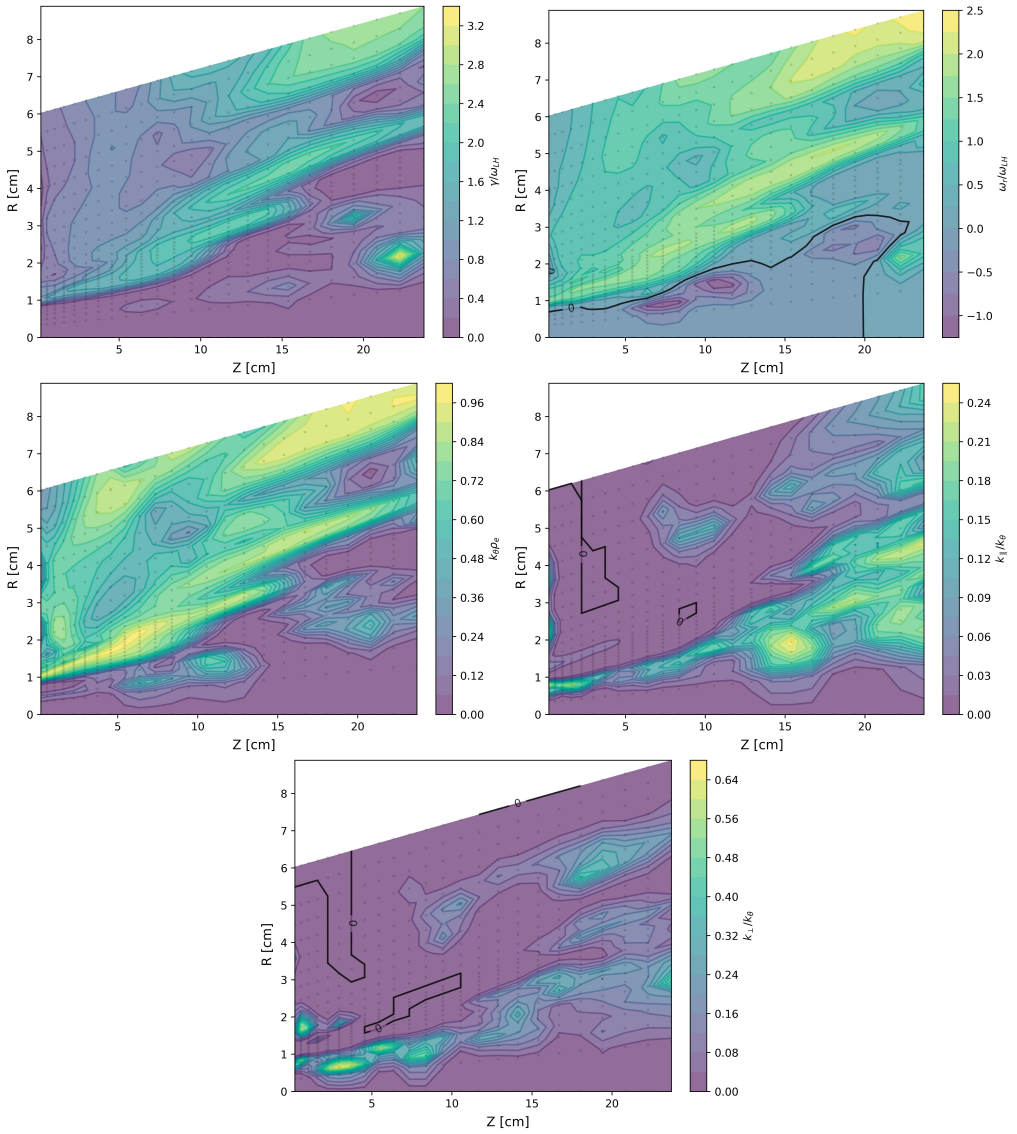

Figure IV.5: 2D maps of γ_{max}, ω^*_{ir} and $\boldsymbol{k}^*$ resulting from a point-wise local analysis across the MN plume region in the collisionless limit.

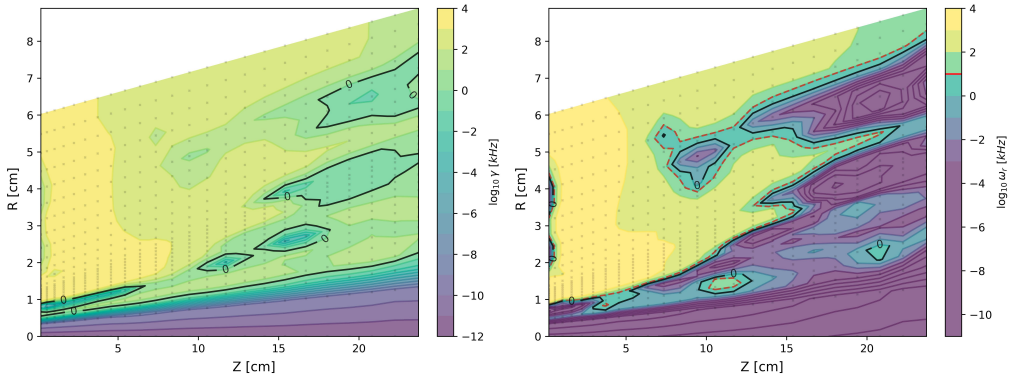

Figure IV.6: 2D maps of γ_{max} and ω^*_{ir} in kHz across the MN plume region in the collisionless case. Black line represents the 1 kHz contour line.

Figure IV.6 shows the same 2D maps for γ_{max} and ω_{ir}^*, this time expressed in kHz. Most of the instabilities and their associated real frequencies fall in the 1 kHz—1 MHz range, decreasing as we move from the near-plume to far-plume region of the discharge. The modes with larger γ_{max} have a mainly-azimuthal associated wavenumber, $\boldsymbol{k}^* \simeq k_\theta^* \mathbf{1}_\theta$.

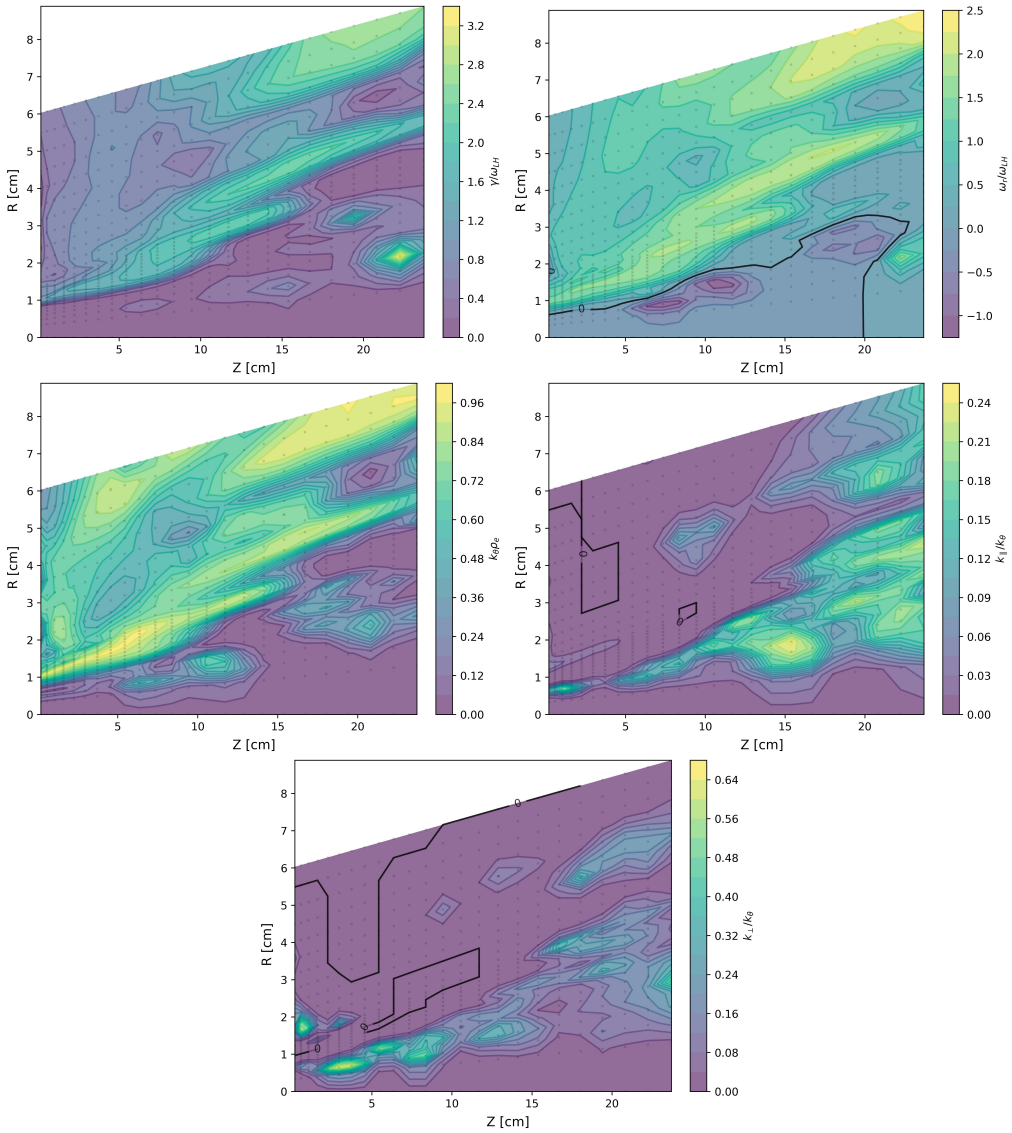

Figure IV.7: 2D maps of γ_{max}, ω_{ir}^* and $\boldsymbol{k}^*$ across the MN plume region in the collisional case.

The effect of collisions on the instability peaks are negligible, as electron-neutral collision frequencies remain in the order $\nu_e \leqslant O(\omega_{LH})$, barely affecting the $O(\omega_{LH})$ growth rates, as shown in Figure IV.7. Overall, the 2D maps of γ_{max}, ω_{ir}^* and $\boldsymbol{k}^*$ remain almost unchanged moving from the collisionless to the collisional case, as the most unstable modes are of the drift-gradient type.

The inclusion of parallel gradients in the dispersion relation plays a major role in the stability of the solution. Their presence allows the onset of instabilities in those points of the nozzle where the MSHI criterion from equation (III.9) does not hold, even without $k_\parallel \neq 0$. This statement is further illustrated by the plots of Figure IV.8, which have been computed by using a form of equation (II.39) *without* parallel gradients, $\nabla_\parallel \ln Q_{e0} = 0$. These plots present a substantially different map for γ_{max}, with the majority of the instabilities taking place in those regions satisfying the MSHI criterion. The map of k_θ^* shows milder peaks, loosely following the ones of γ_{max}. $k_\parallel^*$ has a much more prominent role in the onset of instabilities: this is due to the fact that, in the absence of parallel gradients, $R_\parallel \propto k_\parallel^2$. In the regions where the MSHI

criterion is not satisfied, then, instabilities can only be driven by finite parallel propagation i.e. $k_{\parallel} \neq 0$.

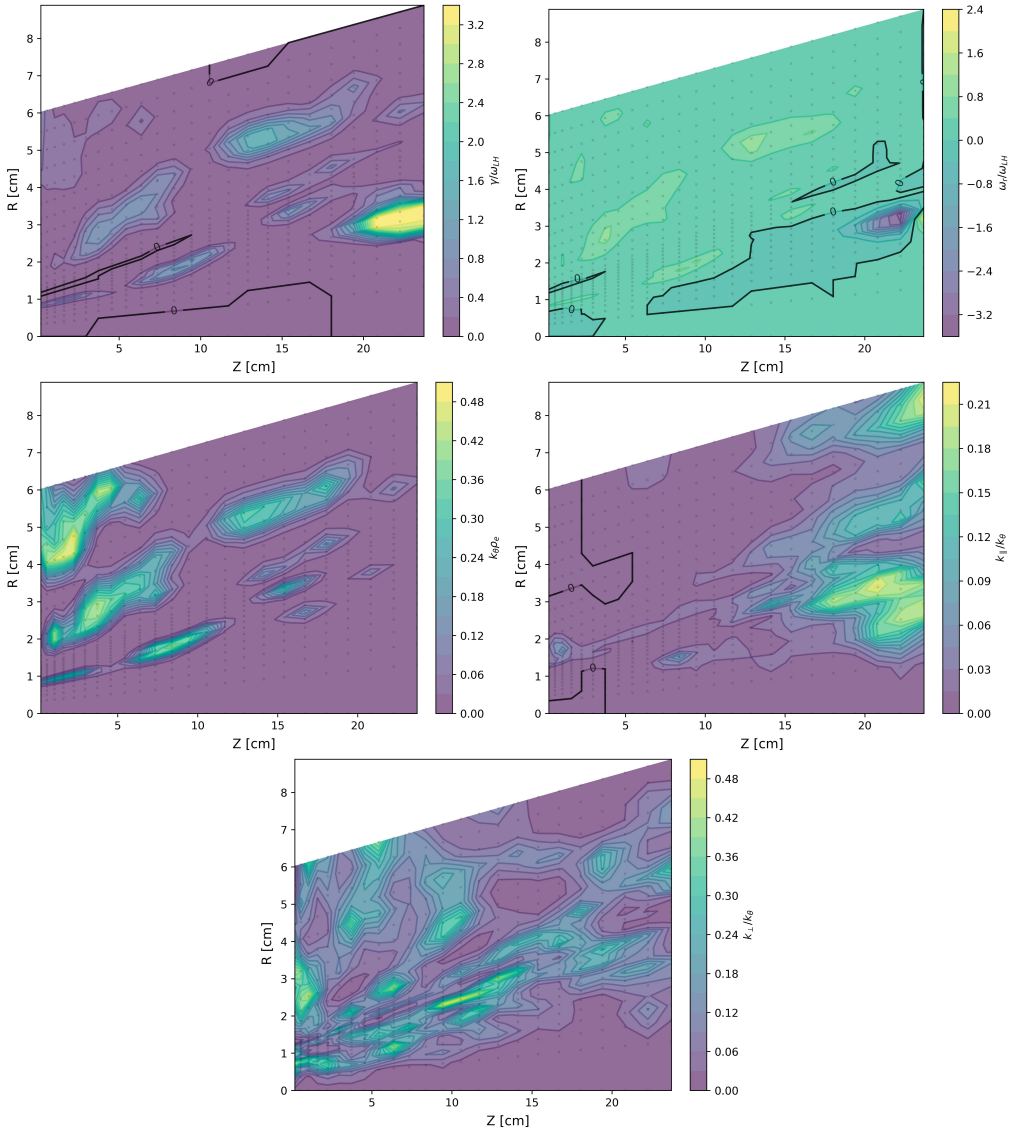

Figure IV.8: 2D maps of γ_{max}, ω_{ir}^* and $\boldsymbol{k}^*$ resulting from a point-wise local analysis across the MN plume region in the collisionless limit neglecting parallel gradients.

We conclude this section with a qualitative comparison with the avaialble experimental data. Recalling Figure IV.5 and IV.6, we have shown that the most unstable modes predicted by our model consist of mainly-azimuthal waves with associated real oscillation frequency ω_{ir}^* in the 1 kHz—1 MHz range. While Hepner et al.[29] and Vinci[30] do find fluctuations in a similar frequency range, they both describe waves with combined axial-azimuthal propagation (where the presence of a large $k_{\parallel}$ introduces kinetic effects which elude our fluid model). Among the cited experimental works, our predicted unstable modes seem to more qualitatively describe fluctuations observed by Takahashi et al.[32] and Maddaloni et al.,[28] which fall in the 10-100 kHz range and consist of mostly azimuthal waves.

V. Summary

We have derived a model to study local linear stability of 3D electrostatic isothermal waves in a partially magnetized plasma presenting inhomogeneities in both parallel and perpendicular directions of the magnetic field, taking into account magnetic curvature effects, parallel dynamics, gyroviscosity and inertial effects

from a fluid perspective. The equilibrium plasma temperature have been assumed to be isotropic.

The presented model is based on expansions of the momentum and continuity equations in the small term $\epsilon = \rho_e/L$, showing the detailed of the dispersion relation in the Low Frequency regime, that is, $\omega_e = O(\omega_{ce}\ \epsilon)$. Our proposed novel matrix approach is particularly convenient for assessing the effect of plasma inhomogeneities by iteratively including larger powers of ϵ.

From this analysis, we have provided simple and general instability criteria for both drift-gradient and drift-dissipative instabilities, highlighting the role of each drift and their interplay in the onset of drift-driven unstable oscillations and the effect of finite Larmor radius effects on the onset/quenching of exponential growth.

As a final step, the dispersion relation has been specialized to the study of the Magnetic Nozzle of an Helicon Thruster, using the data from [36] as a reference. Maps of growth rate, real oscillation frequency and wavenumber have been provided for the most unstable modes predicted to arise in the Magnetic Nozzle, showing the onset of mostly azimuthal instabilities in the 1 kHz—1 MHz range. These findings are in qualitative agreement with some of the available experimental data. The analysis has highlighted the importance of including parallel inhomogeneities in the formulation of the dispersion of an $E \times B$ plasma discharge such as that of a Magnetic Nozzle, as these gradients may drive instabilities even when conditions for MSHI are not met and in the absence of an axially propagating wave, and the absence of important collisional efffects.

However, for this model fluid model to be valid we are intrinsically limited to the study of long wavelengths, $k\rho_e < 1$, and small parallel propagation, $|c_e k_\parallel| < |\omega_e|$. To overcome these limitations, a more consistent as well as complex kinetic approach could be employed.

This work represents a first step in a general formulation of local linear fluid instabilities in MNs and their effects on anomalous electron transport. Future steps include the addition of a quasilinear analysis to gauge the second-order effect of oscillations on transport as well as presenting the derivation of the dispersion relation relevant for the High Frequency regime.

Acknowledgments

This project has received funding from the European Research Council (ERC) under the European Union's Horizon 2020 research and innovation programme (grant agreement No 950466).

A. Gyroviscous Tensor Divergence

From the definition of the gyroviscous tensor , assuming isotropic temperature $T_{e\perp} = T_{e\parallel}$ and fast-ordering dynamics:[41]

$$
\begin{aligned}
-\frac{\nabla\cdot\Pi_e}{m_e n_e} = \frac{1}{e n_e}\Bigg[&\nabla\times\left(\frac{T_e n_e}{B}\mathbf{1}_\parallel\right)\cdot\nabla\boldsymbol{u}_e - \frac{\nabla}{2}\left(\frac{T_e n_e}{B}\mathbf{1}_\parallel\cdot\nabla\times\boldsymbol{u}_e\right) + \\
&+ B\mathbf{1}_\parallel\cdot\nabla\left(\frac{T_e n_e}{B^2}\left(3\mathbf{1}_\parallel\times\mathbf{1}_\parallel\cdot\nabla\boldsymbol{u}_e + \mathbf{1}_\parallel\times\mathbf{1}_\parallel\times\nabla\times\boldsymbol{u}_e + \mathbf{1}_\parallel\cdot\frac{\nabla\times\boldsymbol{u}_e}{2}\mathbf{1}_\parallel\right)\right) + \\
&- \nabla\times\left(\frac{T_e n_e}{B}\left(\mathbf{1}_\parallel\cdot\nabla\boldsymbol{u}_e + \frac{\mathbf{1}_\parallel}{2}\left(\nabla\cdot\boldsymbol{u}_e - 3\mathbf{1}_\parallel\cdot\nabla\boldsymbol{u}_e\cdot\mathbf{1}_\parallel\right)\right)\right)\Bigg]\ ; \quad \text{(A.1)}
\end{aligned}
$$

we can obtain at the 1st order, assuming $\boldsymbol{u}_{e0} \simeq u_{e\theta 0}\mathbf{1}_\theta$ and neglecting $O(\rho_e^2/L^2)$ terms:

$$
\begin{aligned}
\left(-\frac{\nabla\cdot\Pi_e}{m_e n_e}\right)_{\perp 1} = \frac{c_e^2}{\omega_{ce}}\Bigg\{&\left[\frac{k_\perp^2 + k_\theta^2 + 2k_\parallel^2}{2} - ik_\perp\left(\nabla_\perp\ln u_{e\theta 1} + \frac{1}{2}\nabla_\perp\ln\left(\frac{p_{e0}}{B^2}\right)\right)\right. \\
&\left. - 2ik_\parallel\left(\nabla_\parallel\ln u_{e\theta 1} + \frac{1}{2}\nabla_\parallel\ln\left(\frac{p_{e0}}{B^3}\right)\right)\right]u_{e\theta 1} - i\frac{ik_\theta}{2}\nabla_\perp\ln\left(\frac{p_{e0}}{B^2}\right)u_{e\perp 1} \\
&- ik_\theta\left[ik_\parallel + \nabla_\parallel\ln u_{e\parallel 1} + \frac{1}{2}\nabla_\parallel\ln\left(\frac{p_{e0}^2}{B^5}\right)\right]u_{e\parallel 1}\Bigg\} \\
&- i\frac{c_e^2}{2\omega_{ce}}\left(k_\perp\nabla_\perp + 2k_\parallel\nabla_\parallel\right)u_{e\theta 0}\frac{p_{e1}}{p_{e0}} \quad \text{(A.2a)}
\end{aligned}
$$

$$\left(-\frac{\nabla\cdot\Pi_e}{m_e n_e}\right)_{\theta 1} = \frac{c_e^2}{\omega_{ce}}\Bigg\{-\Bigg[\frac{k_\perp^2+k_\theta^2+2k_\parallel^2}{2} - ik_\perp\left(\nabla_\perp \ln u_{e\perp 1} + \frac{1}{2}\nabla_\perp \ln\left(\frac{p_{e0}}{B^2}\right)\right) - 2ik_\parallel\left(\nabla_\parallel \ln u_{e\perp 1} + \frac{1}{2}\nabla_\parallel \ln\left(\frac{p_{e0}}{B}\right)\right)\Bigg] u_{e\perp 1} - i\frac{ik_\theta}{2}\nabla_\perp \ln\left(\frac{p_{e0}}{B^2}\right) u_{e\theta 1} + i\left[k_\perp\left(ik_\parallel + \nabla_\parallel \ln u_{e\parallel 1} + \frac{1}{2}\nabla_\parallel \ln\left(\frac{p_{e0}^2}{B^5}\right)\right) + k_\parallel\left(\nabla_\perp \ln u_{e\parallel 1} + \nabla_\perp \ln B\right)\right] u_{e\parallel 1}\Bigg\} + i\frac{c_e^2}{2\omega_{ce}}\left(k_\theta \nabla_\perp u_{e\theta 0}\right)\frac{p_{e1}}{p_{e0}} \quad \text{(A.2b)}$$

$$\left(-\frac{\nabla\cdot\Pi_e}{m_e n_e}\right)_{\parallel 1} = \frac{ic_e^2}{\omega_{ce}}\Bigg\{k_\theta\left[ik_\parallel + \nabla_\parallel \ln u_{e\perp 1} + \frac{1}{2}\nabla_\parallel \ln B\right] u_{e\perp 1} - \left[k_\perp\left(ik_\parallel + \nabla_\parallel \ln u_{e\theta 1} + \frac{1}{2}\nabla_\parallel \ln B\right) + k_\parallel\left(\nabla_\perp \ln u_{e\theta 1} + \nabla_\perp \ln\left(\frac{p_{e0}}{B^3}\right)\right)\right] u_{e\theta 1} - k_\theta \nabla_\parallel \ln\left(\frac{p_{e0}}{B^4}\right) u_{e\parallel 1}\Bigg\} - i\frac{c_e^2}{2\omega_{ce}}\left(k_\perp \nabla_\parallel u_{e\theta 0}\right)\frac{p_{e1}}{p_{e0}}\,. \quad \text{(A.2c)}$$

References

[1]H.R. Kaufman. Technology of closed-drift thrusters. *AIAA Journal*, 23:78–87, 1985.

[2]D.M. Goebel and I. Katz. *Fundamentals of Electric Propulsion: Ion and Hall Thrusters*. Jet Propulsion Laboratory, Pasadena, CA, 2008.

[3]Eduardo Ahedo. Plasmas for space propulsion. *Plasma Physics and Controlled Fusion*, 53(12):124037, 2011.

[4]J Navarro-Cavallé, M Wijnen, P Fajardo, and E Ahedo. Experimental characterization of a 1 kw helicon plasma thruster. *Vacuum*, 149:69–73, 2018.

[5]Danis Packan, Paul-Quentin Elias, Julien Jarrige, Theo Vialis, Sara Correyero, Simon Peterschmitt, J.C. Porto-Hernandez, Mario Merino, Álvaro Sánchez-Villar, Eduardo Ahedo, G. Peyresoubes, A. Thorinius, S. Denis, Kristoff Holste, Peter Klar, S. Scharmann, J. Zorn, M. Bekemans, T. Scalais, E. Bourguignon, S. Zurbach, P. Azais, I. Habbassi, Magali Mares, and Andy Hoque. H2020 MINOTOR: Magnetic nozzle electron cyclotron resonance thruster. In 36^{th} *International Electric Propulsion Conference*, number IEPC-2019-875, Vienna, Austria, 2019. Electric Rocket Propulsion Society.

[6]Mario Merino and Eduardo Ahedo. Magnetic nozzles for space plasma thrusters. In J. Leon Shohet, editor, *Encyclopedia of Plasma Technology*, volume 2, pages 1329–1351. Taylor and Francis, 2016.

[7]Igor D. Kaganovich, Andrei Smolyakov, Yevgeny Raitses, Eduardo Ahedo, Ioannis G. Mikellides, Benjamin Jorns, Francesco Taccogna, Renaud Gueroult, Sedina Tsikata, Anne Bourdon, Jean-Pierre Boeuf, Michael Keidar, Andrew Tasman Powis, Mario Merino, Mark Cappelli, Kentaro Hara, Johan A. Carlsson, Nathaniel J. Fisch, Pascal Chabert, Irina Schweigert, Trevor Lafleur, Konstantin Matyash, Alexander V. Khrabrov, Rod W. Boswell, and Amnon Fruchtman. Perspectives on physics of exb discharges relevant to plasma propulsion and similar technologies. *Physics of Plasmas*, 27(12):120601, 2020.

[8]R.J. Hastie, J.J. Ramos, F. Porcelli, M.I. of T.P. Science, and F. Center. Drift ballooning instabilities in tokamak edge plasmas. *Physics of Plasmas*, 10(11):4405–4412, 2003.

[9]E. Ahedo and J. Ramos. Parametric analysis of the two-fluid tearing instability. In *50th Annual Meeting of the APS-Division of Plasma Physics, November 2008*, 2008.

[10]J. J. Ramos. Normal-mode-based theory of collisionless plasma waves. *Journal of Plasma Physics*, 2019.

[11]J. J. Ramos, E. Bello-Benítez, and E. Ahedo. Local analysis of electrostatic modes in a two-fluid E x B plasma. *Physics of Plasmas*, 28(5):052115, 2021.

[12]K. Hara, A. R. Mansour, A. C. Denig, and S. Tsikata. Fluid and kinetic plasma instabilities for hall effect thrusters. In *37th International Electric Propulsion Conference*, 2022.

[13]Jean-Pierre Boeuf and Andrei Smolyakov. Physics and instabilities of low-temperature e× b plasmas for spacecraft propulsion and other applications. *Physics of Plasmas*, 30(5), 2023.

[14]E. Ahedo. Using electron fluid models to analyze plasma thruster discharges. *Journal of Electric Propulsion*, 2(1):2, 2023.

[15]E. Choueiri. Plasma oscillations in Hall thrusters. *Physics of Plasmas*, 8(4):1411–1426, 2001.

[16]Diego Escobar and Eduardo Ahedo. Low frequency azimuthal stability of the ionization region of the hall thruster discharge. i. local analysis. *Physics of Plasmas*, 21(4):043505, 2014.

[17]E. Bello-Benítez and E. Ahedo. Axial-azimuthal, high-frequency modes from global linear-stability model of a Hall thruster. *Plasma Sources Science and Technology*, 30(3):035003, mar 2021.

[18]Davide Poli, Enrique Bello-Benítez, Pablo Fajardo, and Eduardo Ahedo. Time-dependent axial fluid model of the hall thruster discharge and its plume. *Journal of Physics D: Applied Physics*, 2023.

[19]Enrique Bello-Benítez, Alberto Marín-Cebrián, and Eduardo Ahedo. Effect of injection conditions on the non-linear behavior of the ECDI and related turbulent transport, 2024. Pre-print available at https://arxiv.org/pdf/2405.08761.

[20]A.I. Morozov, Y.V. Esipchuk, A.M. Kapulkin, V.A. Nevrovskii, and V.A. Smirnov. Effect of the magnetic field on a closed-electron-drift accelerator. *Sov. Phys.-Tech. Phys.(Engl. Transl.) 17: No. 3, 482-7 (Sep 1972).*, 1972.

[21]Y.V. Esipchuk and G.N. Tilinin. Drift instability in a Hall-current plasma accelerator. *Sov. Physics-Tech. Physics*, 21(4):417–423, 1976.

[22]W. Frias, A.I. Smolyakov, I.D. Kaganovich, and Y. Raitses. Long wavelength gradient drift instability in Hall plasma devices. I. Fluid theory. *Physics of Plasmas*, 19:072112, 2012.

[23]A.I. Smolyakov, O. Chapurin, W. Frias, O. Koshkarov, I. Romadanov, T. Tang, M. Umansky, Y. Raitses, I.D. Kaganovich, and V.P. Lakhin. Fluid theory and simulations of instabilities, turbulent transport and coherent structures in partially-magnetized plasmas of ExB discharges. *Plasma Physics and Controlled Fusion*, 59:014041, 2017.

[24]A.A. Litvak and N.J. Fisch. Resistive instabilities in Hall current plasma discharge. *Physics of Plasmas*, 8(2):648–651, 2001.

[25]O. Buneman. Instability of electrons drifting through ions across a magnetic field. *Journal of Nuclear Energy. Part C, Plasma Physics, Accelerators, Thermonuclear Research*, 4(2):111–117, 1962.

[26]N. A. Krall and P. C. Liewer. Low-frequency instabilities in magnetic pulses. *Physical Review A*, 4:2094–2103, 1971.

[27]Kazunori Takahashi, Christine Charles, and Rod W Boswell. Wave-driven electron inward transport in a magnetic nozzle. *Scientific reports*, 12(1):20137, 2022.

[28]Davide Maddaloni, Jaume Navarro-Cavallé, Mario Merino, and Filippo Terragni. Experimental investigation of oscillations in a magnetic nozzle. In 35^{th} *International Conference on Plasmas and Ionized Gases*, Egmond aan Zee, The Netherlands, July 9–14, 2023.

[29]Shadrach Hepner, Benjamin Wachs, and Benjamin Jorns. Wave-driven non-classical electron transport in a low temperature magnetically expanding plasma. *Applied Physics Letters*, 116(26):263502, 2020.

[30]Alfio Emanuele Vinci. *Physics of magnetic nozzles and helicon plasma discharges.* PhD thesis, Université d'Orléans, 2022.

[31]T. R. Desjardins and M. Gilmore. Dynamics of flows, flucuations, and global instability under electrode biasing in a linear plasma device. *Physics of Plasmas*, 2016.

[32]K. Takahashi. Thirty percent conversion efficiency from radiofrequency power to thrust energy in a magnetic nozzle plasma thruster. *Scientific Reports*, 12:18618, 2022.

[33]J. D. Huba and C. S. Wu. Effects of a magnetic field gradient on the lower hydrid drift instability. *The Physics of Fluids*, 19(7):988–994, 1976.

[34]P. A. Sturrock. In what sense do slow waves carry negative energy? *Journal of Applied Physics*, 31(11), 1960.

[35]A. Hasegawa. *Plasma Instabilities and Nonlinear Effects.* Springer-Verlag, 1975.

[36]Pedro Jiménez, Jiewei Zhou, Jaume Navarro-Cavallé, Pablo Fajardo, Mario Merino, and Eduardo Ahedo. Analysis of a cusped helicon plasma thruster discharge. *Plasma Sources Science and Technology*, 32(10):105013, 2023.

[37]Pedro Jimenez. Data from: Analysis of a cusped helicon plasma thruster discharge, February 2024.

[38]S.A. Andersen, V.O. Jensen, P. Nielsen, and N. D'Angelo. Continuous supersonic plasma wind tunnel. *Phys. Fluids*, 12(3):557–560, 1969.

[39]Eduardo Ahedo and Mario Merino. Two-dimensional supersonic plasma acceleration in a magnetic nozzle. *Physics of Plasmas*, 17(7):073501, 2010.

[40]Jiewei Zhou, Gonzalo Sánchez-Arriaga, and Eduardo Ahedo. Time-dependent expansion of a weakly-collisional plasma beam in a paraxial magnetic nozzle. *Plasma Sources Science and Technology*, 30(4):045009, 2021.

[41]J.J. Ramos. General expression of the gyroviscous force. *Physics of Plasmas*, 12(11):112301, 2005.

[42]Thomas H Stix. *Waves in plasmas.* Springer Science & Business Media, 1992.

[43]J. Vranjes and S. Poedts. The universally growing mode in the solar atmosphere: coronal heating by drift waves. *Monthly Notices of the Royal Astronomical Society*, 2009.

[44]J. Zhou, A. Domínguez-Vázquez, P. Fajardo, and E. Ahedo. Magnetized fluid electron model within a two-dimensional hybrid simulation code for electrodeless plasma thrusters. *Plasma Sources Science and Technology*, 31(4):045021, 2022.

[45]J. Perales-Díaz, A. Domínguez-Vázquez, P. Fajardo, E. Ahedo, F. Faraji, M. Reza, and T. Andreussi. Hybrid plasma simulations of the HT5k thruster. In *ExB Plasmas Workshop, Young researchers "poster" mini-session*, Madrid, Spain, February 16-18, 2022.